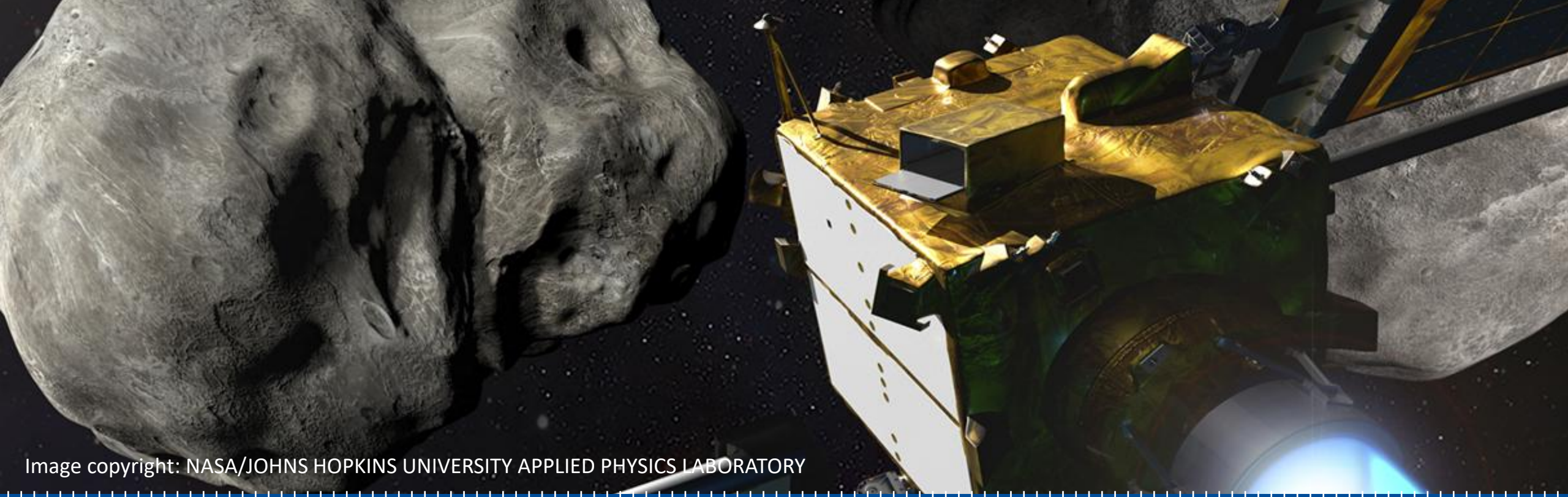

ANALYSIS OF ASTEROID DEFLECTION MISSION OPTIONS FOR THE 2025 PLANETARY DEFENSE CONFERENCE HYPOTHETICAL ASTEROID IMPACT THREAT SCENARIO BY THE ITALIAN SPACE AGENCY DELEGATION AT SMPAG

S. Franzese, E. Basile, E. M. Polli, C. Colombo, P. Vasiliki, M. Castronuovo, J. L. Cano

POLITECNICO MILANO 1863

Planetary Defence Conference 2025 - 6th May 2025

Outline

- RECONNAISSANCE MISSION
  - Epoch 1: Scenario Description and reconnaissance
  - Epoch 2: Scenario description
- DEFLECTION MISSIONS
  - Deflection strategies & Optimisation framework
  - Multiple Kinetic Impactor strategy
  - Rendezvousing deflection strategies
- CONCLUSION
  - Key findings and TRL considerations

RECONNAISSANCE MISSION

Epoch 1: scenario description and reconnaissance

Impact threat scenario

IAWN warning on 1st August 2024 → Epoch 1 [1]

- **S-type asteroid** with diameter range: $50 - 280$ m.
- Close encounter date: **24th April 2041 →** $t_w \approx 16.5$ years.
- **Full length of impact risk chord →** $C = 21850$ km.

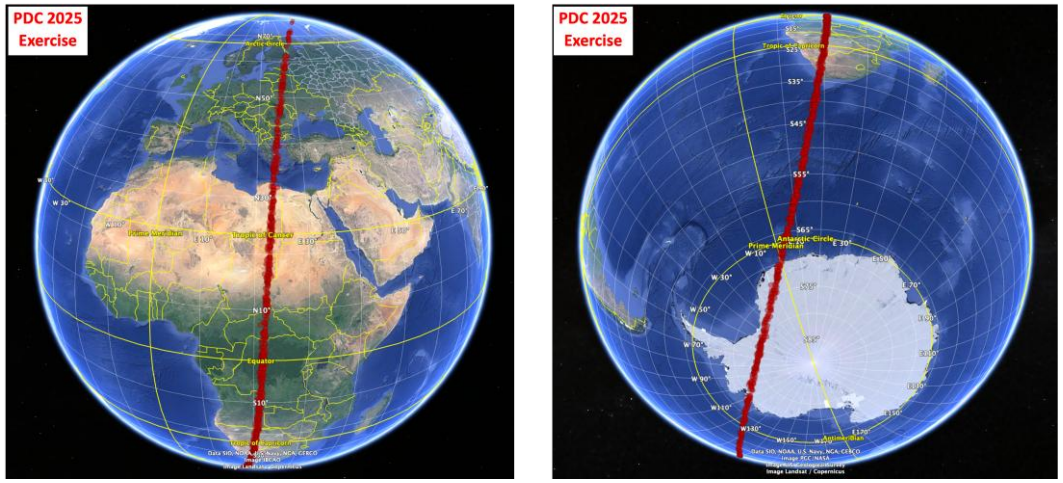

Asteroid 2024 PDC25 risk corridor at Epoch 1 [1].

Flyby reconnaissance mission

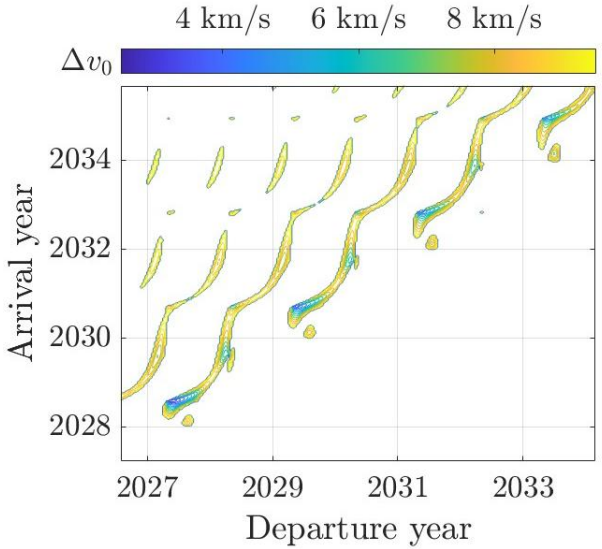

Grid-search approach.

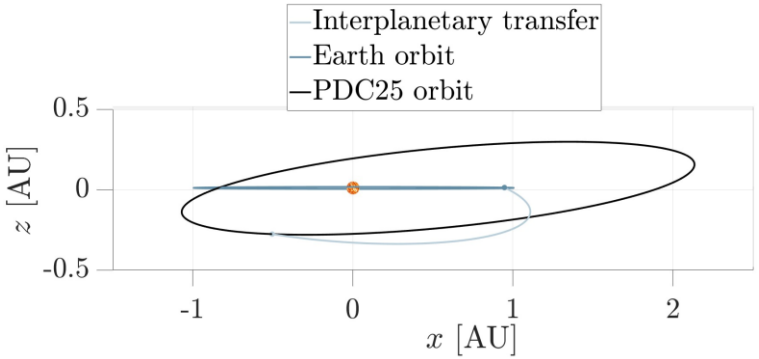

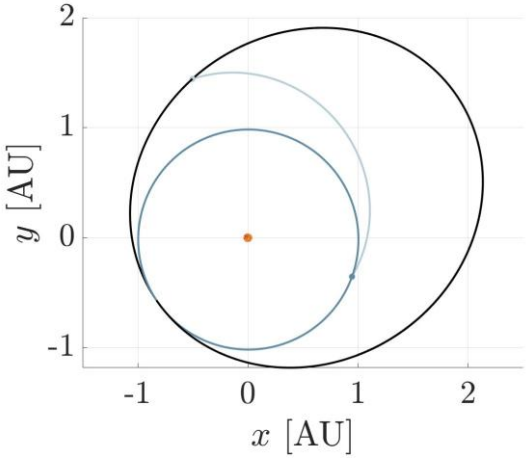

Flyby reconnaissance mission.

Departure date
2^{nd} September 2027

Arrival date
31^{st} March 2028

[1] NASA/JPL CNEOS, 2024. URL: https://cneos.jpl.nasa.gov/pd/cs/pdc25/.

Epoch 2: scenario description

Flyby data available on May 2028 → Epoch 2 [1]

- **S-type asteroid** with diameter range: $145 - 155$ m.
- Close encounter date: **24th April 2041 →** $t_w \approx 13$ years.
- Probability of **impact** with Earth: **100 %**

Keplerian Element	Value
Semi-major axis (a)	1.67634 AU
Eccentricity (e)	0.3999
Inclination (i)	10.868°
Right Ascension of the Ascending Node (Ω)	214.288°
Argument of pericentre (ω)	0.168°
True anomaly (ϑ)	359.373°

Epoch 2: Keplerian elements 10 hours before MOID [2].

Northward b-plane deflection:
7370 km ≈ 34 % C ≈ 1.16 R_E

Southward b-plane deflection:
15352 km ≈ 70 % $C \approx 2.41$ R_E

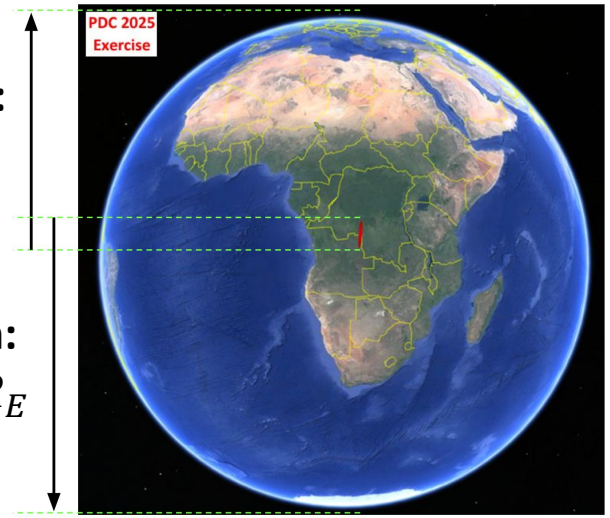

Asteroid 2024 PDC25 deflection requirements at Epoch 2 [1].

[1] NASA/JPL CNEOS, 2024. URL: https://cneos.jpl.nasa.gov/pd/cs/pdc25/.
[2] NASA JPL Horizons, 2024. URL: https://ssd.jpl.nasa.gov/horizons/.

DEFLECTION MISSIONS

Deflection strategies & Optimisation framework

Impulsive strategies	Slow push/pull strategies
Multiple Kinetic Impactor (MKI)	Gravity Tractor: Standard (GT) and Enhanced (EGT)
Nuclear Explosive Devices (NEDs)	Laser Ablation: Single (SLA) and Multiple (MLA)
	Ion Beam Deflection: Single (SIDB) and Multiple (MIBD)

Departure conditions

- **Launcher: Falcon 9 Heavy Expendable** → maximum m_{s/c_0} compliant with $C_3 \leq 25\ km^2/s^2$ [3].
- **Launch window opens 1st June 2029** → ≈ 1.5 years after arrival of fly-by reconnaissance mission.

Optimisation framework

Competing objectives [4]

- Maximising **deflection** performance
- Minimising **warning time**
- Minimising total **launch mass**

Fragmentation avoidance requirement → $\delta v \leq 4 - 10\%\ v_{esc}$

Feasible spacecraft design

[3] NASA Launch Services Program, 2025. URL: https://elvperf.ksc.nasa.gov/Pages/Default.aspx.

[4] J. P. Sanchez, C. Colombo, M. Vasile, G. Radice, Journal of Guidance, Control, and Dynamics, vol. 32, no. 1, pp. 121–142, 2009. DOI: https://doi.org/10.2514/1.36774.

Multiple Kinetic Impactor strategy

MKI nominal mission

Mean properties

Southward b-plane deflection distance:
$15352\ \text{km} \approx 70\ \%\ C \approx 2.41\ R_E$

Physical property	Assumption	Value [1]
Density	Mean density	2224.07 kg/m^3
Size	Mean equivalent diameter	150.01 m
Mass	Equivalent sphere	$3.96677 \cdot 10^9$ kg
Escape velocity	Uniform on the surface	8.40 cm/s
Momentum enhancement	$\beta = 3.61 \frac{\rho}{2400} - 0.03$	3.345

Mean physical properties of asteroid 2024 PDC25.

$\beta = (3.61 \pm 0.2) \frac{\rho}{2400} - 0.03 \pm 0.02$ [5]

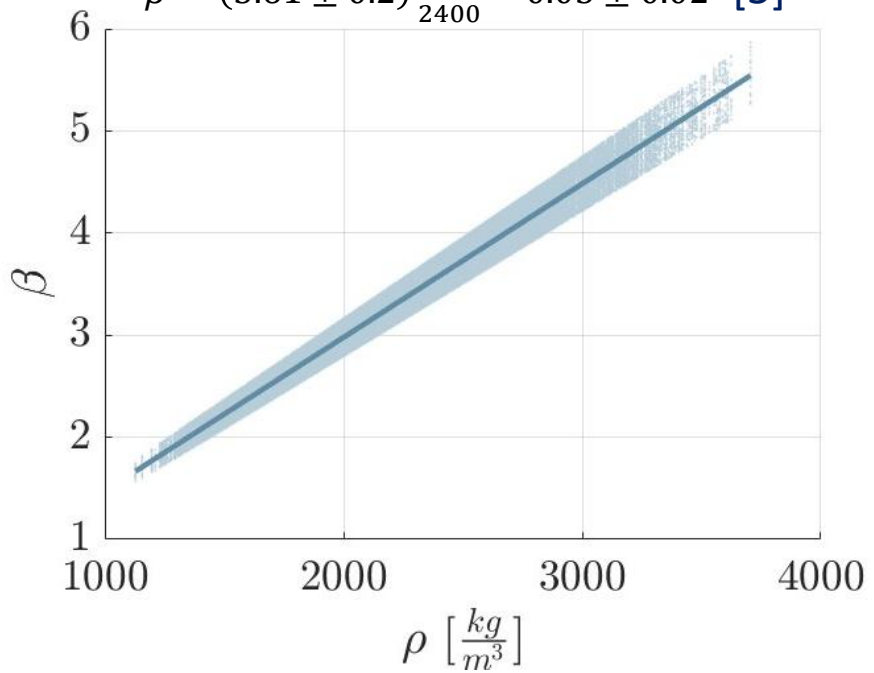

Relation between momentum enhancement and density of asteroid 2024 PDC25.

[1] NASA/JPL CNEOS, 2024. URL: https://cneos.jpl.nasa.gov/pd/cs/pdc25/.

[5] A. F. Cheng, H. F. Agrusa, B. W. Barbee, A. J. Meyer, T. L. Farnham, S. D. Raducan, D. C. Richardson, E. Dotto, A. Zinzi,V. Della Corte, et al., Nature 616 (2023) 457–460. DOI: https://doi.org/10.1038/s41586-023-05878-z.

MKI nominal mission and sensitivity analysis

Three-spacecraft nominal mission

- **Three spacecraft** are sufficient for ensuring the minimum **southwards impact parameter** requirement

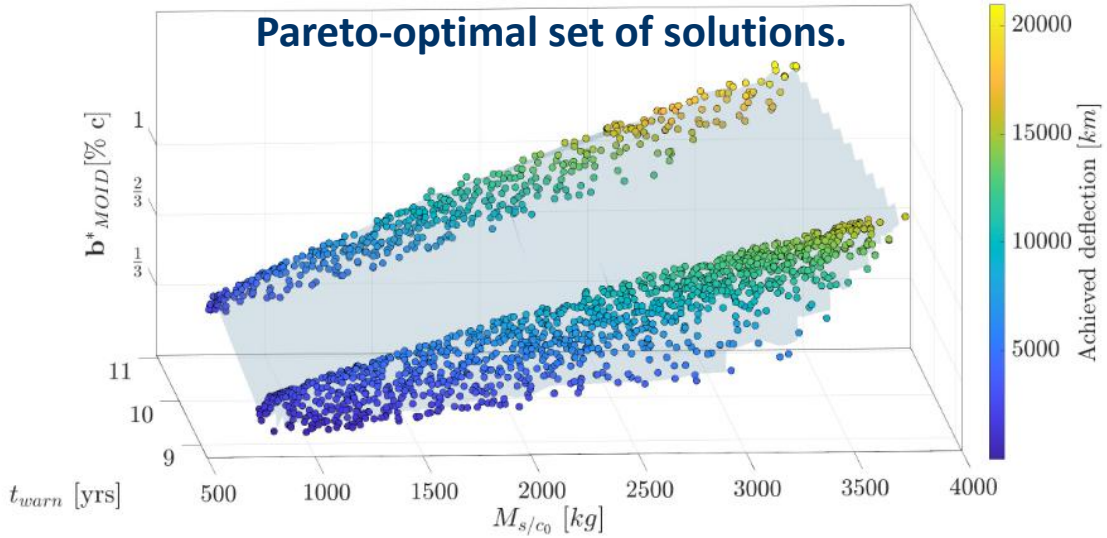

Maximum deflection mission:
b^* = **20955 km**

- Obtained solution has **36.5% margin** over the requirement
- At least 14 days between impacts [6] ✓

Sensitivity analysis

Uncertainty Source	Variables involved	Number of samples
Asteroid's Position	Asteroid position at first impact ($\boldsymbol{r_{imp}}$)	100,000
Relative Navigation Error	Relative velocity at impacts ($\boldsymbol{V_{rel}}$)	200
	Relative position at impact ($\boldsymbol{r_c}$)	1,000
Physical Parameters	Asteroid's mass ($\boldsymbol{M_{ast}}$)	5,000
	Momentum enhancement factor (β)	200

Settings for Monte Carlo analysis.

If requirements satisfied with **2σ confidence level**

Mission is **ROBUST** to perturbations

[6] N. Chabot, E. Adams, A. Rivkin, and J. Kalirai, Acta Astronautica, vol. 220, pp. 118– 125, 2024. DOI: https://doi.org/10.1016/j.actaastro.2024.04.001.

MKI: Sensitivity Analysis

Physical parameters

DATA

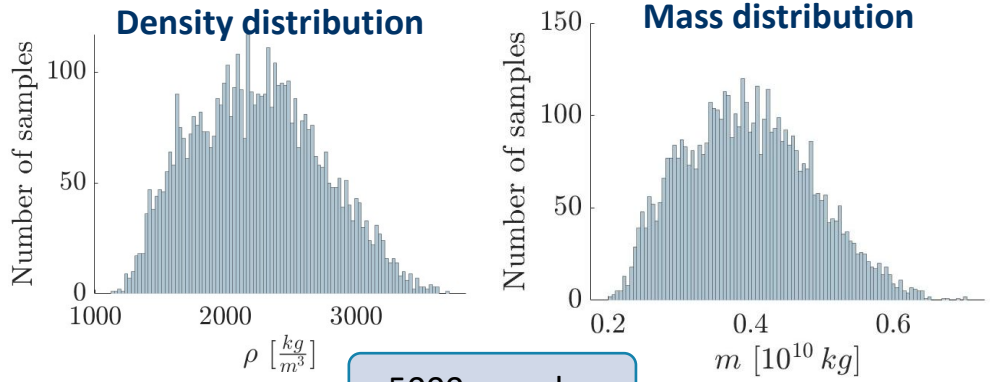

5000 samples

x

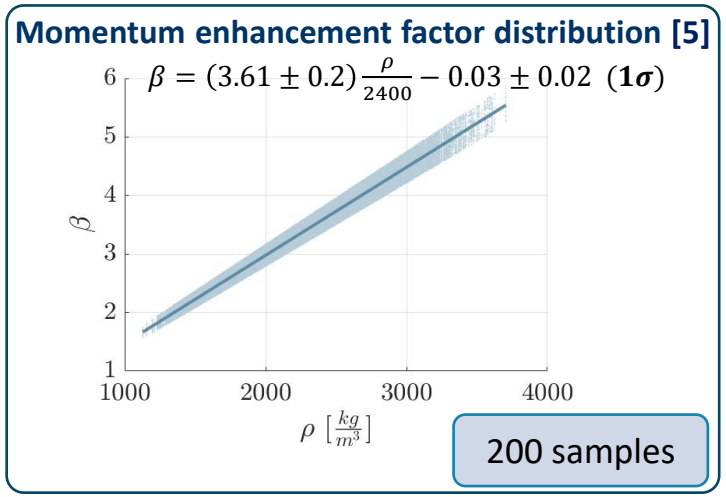

200 samples

=

1'000'000 physical realisations

RESULTS

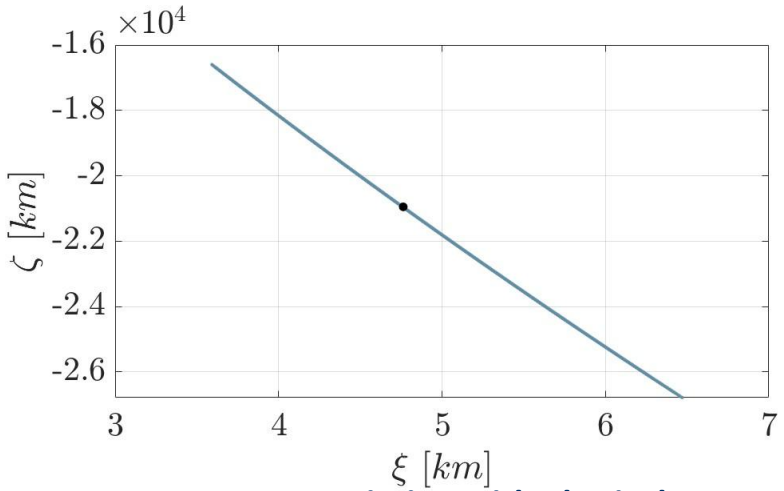

Impact parameter variation with physical properties

- All solutions **compliant** with the **minimum impact parameter** requirement

b^*_{min} = ***16629 km***

Minimum impact parameter requirement: b^*_{south} = ***15352 km***

[5] A. F. Cheng, H. F. Agrusa, B. W. Barbee, A. J. Meyer, T. L. Farnham, S. D. Raducan, D. C. Richardson, E. Dotto, A. Zinzi,V. Della Corte, et al., Nature 616 (2023) 457–460. DOI: https://doi.org/10.1038/s41586-023-05878-z.

MKI: Sensitivity Analysis

Physical parameters

RESULTS

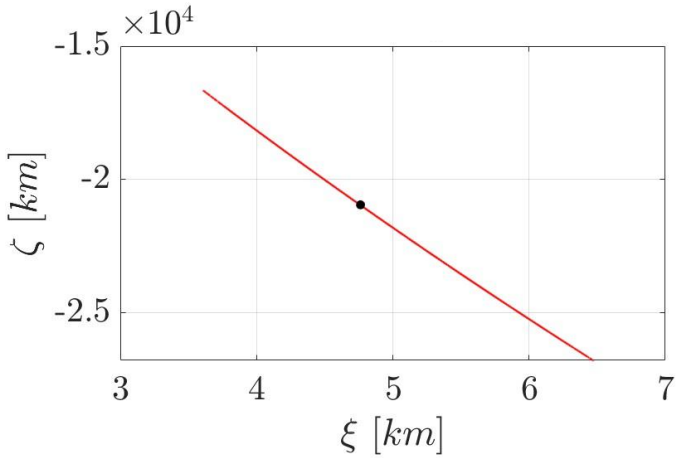

Second impactor.

- **39.76 %** of the realisations do **not** respect the **fragmentation threshold** when considering the second impact

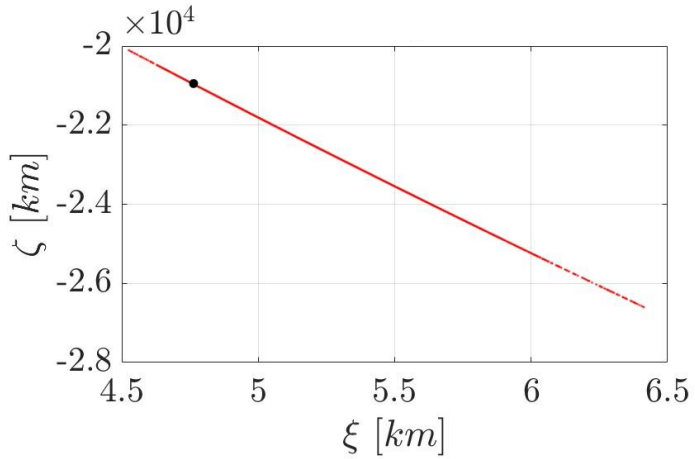

Third impactor.

- The solution does **not** respond **robustly** to the variation of **physical parameters**

Minimum impact parameter requirement: b^*_{south} = ***15352 km***

Robust MKI Mission Design

Six-spacecraft mission

Spacecraft	Launch	DSM	Arrival	c_3 $[km^2/s^2]$	m_{s/c_0} [kg]	$m_{s/c}$ [kg]	V_{rel} [km/s]	b* [km]	Δv
#1	**2030-04-19**	2031-04-21	2032-09-27	14.93 km2/s2	532 kg	288 kg	10.97 km/s	2387 km	3.18 % v_{esc}
#2	2030-04-23	2031-04-15	2032-10-11	16.69 km2/s2	592 kg	453 kg	8.54 km/s	5932 km	3.89 % v_{esc}
#3	2030-04-28	2031-04-14	2032-10-25	14.60 km2/s2	561 kg	440 kg	8.01 km/s	9485 km	3.54 % v_{esc}
#4	2030-05-03	2031-05-17	2032-11-08	14.83 km2/s2	559 kg	451 kg	7.83 km/s	13022 km	3.55 % v_{esc}
#5	2030-05-07	2031-05-15	2032-11-22	17.66 km2/s2	544 kg	310 kg	10.96 km/s	15656 km	3.42 % v_{esc}
#6	2030-05-11	2031-06-10	**2032-12-06**	16.37 km2/s2	441 kg	218 kg	11.44 km/s	**17549 km**	2.51 % v_{esc}

- The robust solution allows for adjustments of the deflection exploiting **successive perihelia**

Trajectory for first impactor.

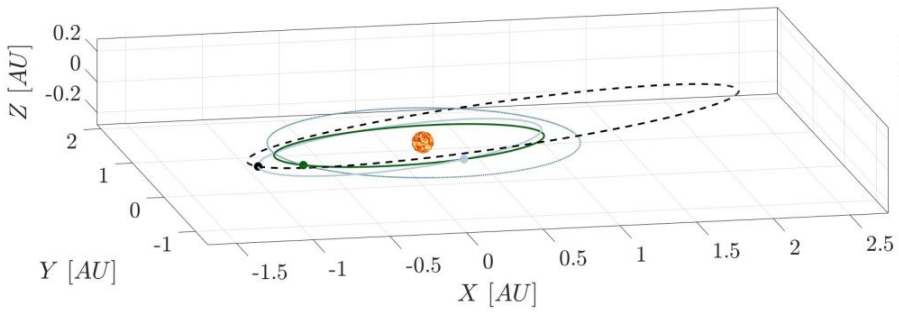

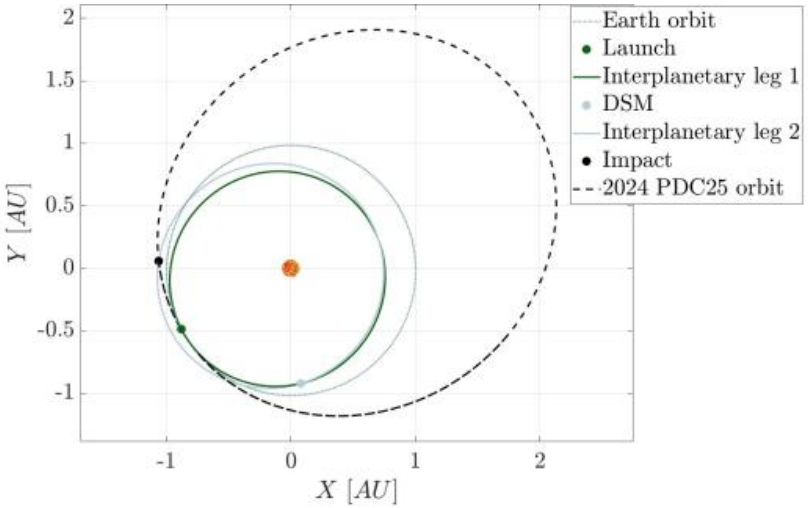

Robust MKI Mission Design

Physical parameters

- **100%** of the samples satisfy the **fragmentation avoidance** requirement
- **97.95%** of the samples satisfy the **minimum impact parameter** requirement

b^*_{min} = ***13813.84 km***

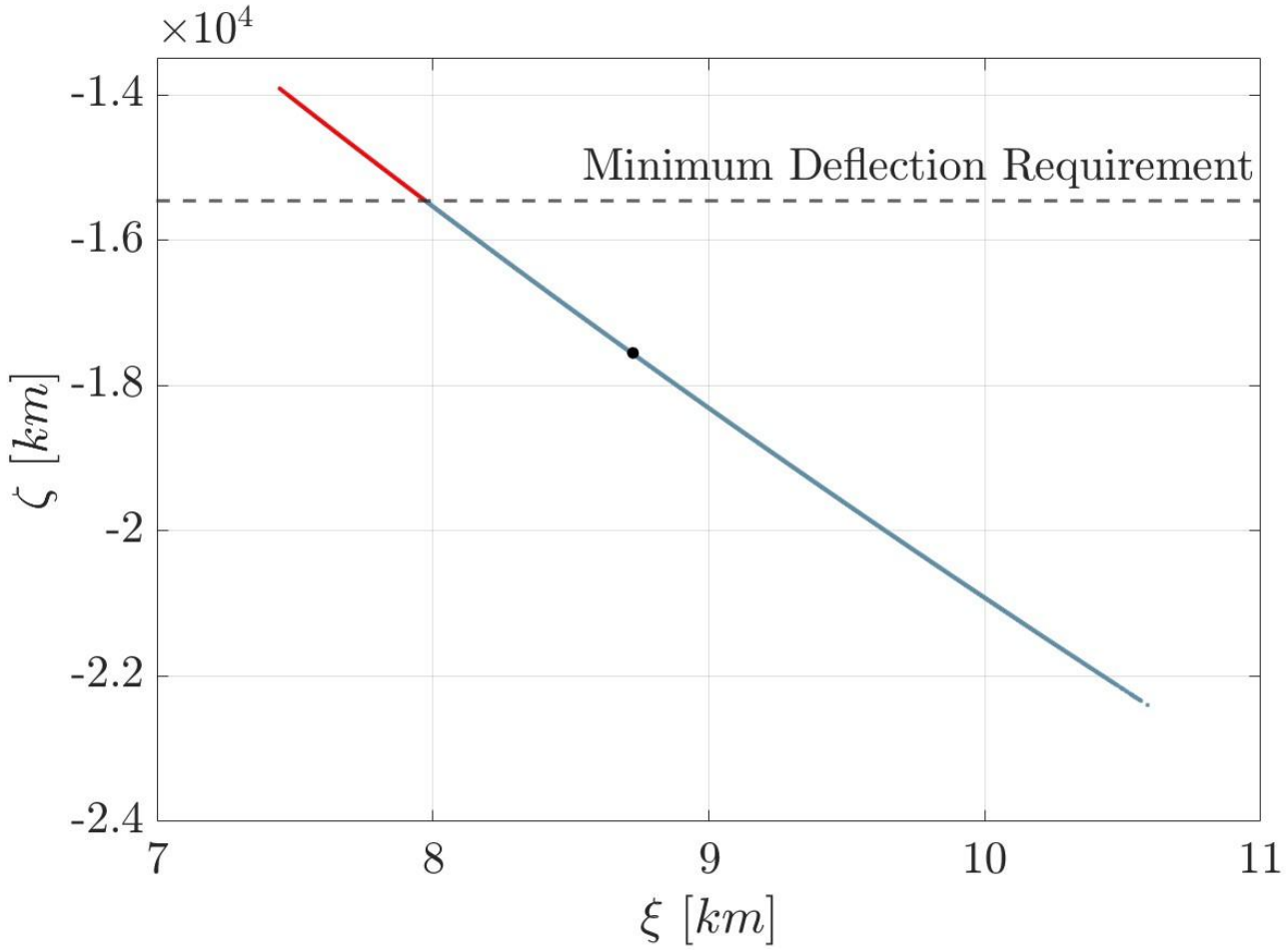

- The remainder **2.05%** includes the **extremes** of the **distributions:**

Highest mass

Lowest momentum enhancement factor

The solution responds **robustly** to physical parameters variation

Rendezvousing deflection strategies

Mission design for rendezvousing strategies

Selected mission
Pareto-optimal solution maximising the deflection.

→ **Time-optimal low-thrust trajectory**

→ **Optimised mission feasibility**

$$m_{str} \geq 0.13\, m_{s/c_0}$$

$$m_{f_{stored}} \leq 0.65\, m_{s/c_0}$$

NEXT-C thrusters used on DART mission [7]

- **High TRL** → Selected for mission design.
- **Thruster efficiency** → $\eta_T = \dfrac{F_{\max_1} I_{sp}\, g_0}{2\, P_{in_1,max}}$

$P_{in_1,max}\ [kW]$	$F_{max_1}\ [N]$	$I_{sp}\ [s]$	$\eta_T\ [-]$	$m_{thr_{dry}}\ [kg]$
7.78	0.235	4190	0.6208	50.00

NEXT-C thrusters main properties used in this study [7].

Mission analysis at Epoch 2 [1]

- S-type → Assumed material: **forsterite (Mg_2SiO_4).**
- **Spherical equivalent diameter:** $145 - 155$ m [1].

	$d_a\ [m]$	$\rho_a\ [kg/m^3]$	$M_a\ [kg]$	$\alpha_s\ [-]$	$v_{esc}\ [cm/s]$
Lowest Mass	147	1211	2.00 E+09	0.221	6.05
50th percentile	150	2207	3.93 E+09	0.179	8.33
Highest Mass	155	3598	7.03 E+09	0.090	10.99

Asteroid 2024 PDC25 percentiles properties at Epoch 2 [1].

[1] NASA/JPL CNEOS, 2024. URL: https://cneos.jpl.nasa.gov/pd/cs/pdc25/.
[7] NASA, 2021. NASA's Evolutionary Xenon Thruster-Commercial (NEXT-C). NASA Technical Reports Server. URL: https://ntrs.nasa.gov/citations/20210024276.

Deflection requirements

Northward b-plane deflection distance:

$$\mathbf{7370\ km \approx 34\ \%\ C \approx 1.16\ R_E}$$

(Includes 125 km asteroid perigee altitude)

2) Successful Northward deflection

NEDs in “Carrier” configuration, IBD, LA and GT can deflect the asteroid in both directions.

Low-thrust deflection missions continue until MOID.

Southward b-plane deflection distance:

$$\mathbf{15352\ km \approx 70\ \%\ C \approx 2.41\ R_E}$$

(Includes 125 km asteroid perigee altitude)

1) Successful Southward deflection

3) Partial Southward deflection

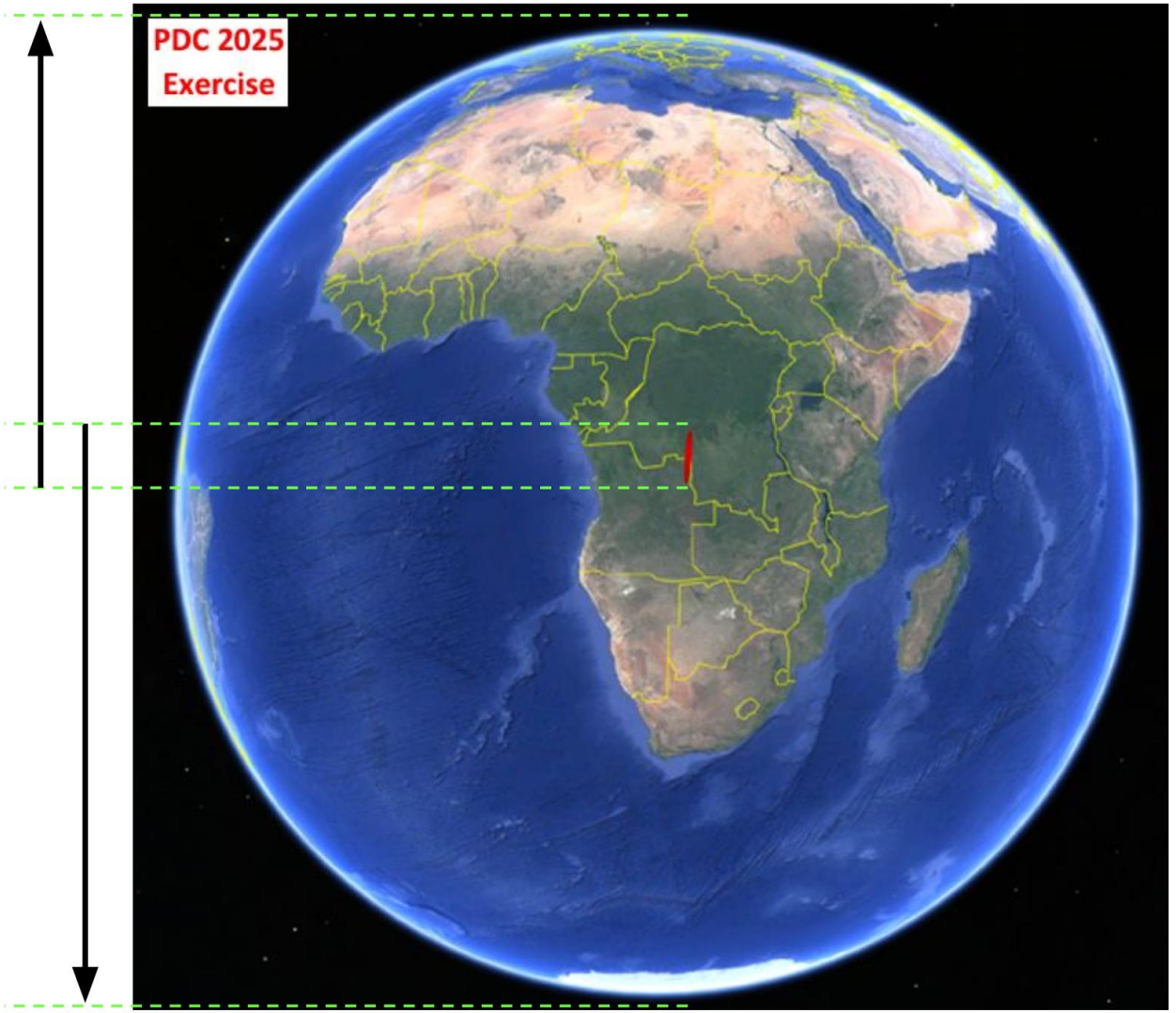

Asteroid 2024 PDC25 deflection requirements at Epoch 2 [1].

[1] NASA/JPL CNEOS, 2024. URL: https://cneos.jpl.nasa.gov/pd/cs/pdc25/.

Stand-off NEDs campaigns – Deflection δb [% C]

- **Arrival constraint** → $4 - 23$ months before perihelion.
- **NEDs detonations:**
  - Far side of the asteroid [8] → Spacecraft shielded.
  - Symmetrically around perihelion.
  - Time separation of 14 days [6].
- The δv_{Nuc} from a nuclear stand-off explosion [4][8]:

$$\delta v_{Nuc} = \delta v_{gamma} + \delta v_{X-rays} + \delta v_{neutrons} + \delta v_{debris}$$

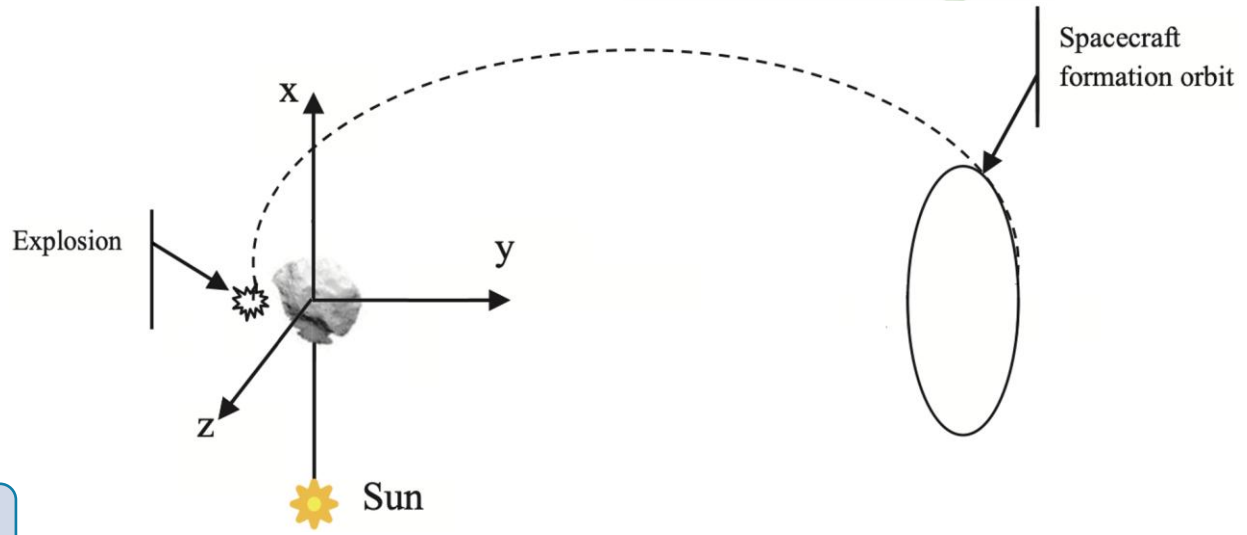

Stand-off detonations in "Carrier" configuration scheme [8].

	Early (2032 Perihelion)		Primary (2034 Perihelion)		Secondary (2037 Perihelion)		Late (2039 Perihelion)
	5 x 0.4 Mt	7 x 0.3 Mt	5 x 0.4 Mt	7 x 0.3 Mt	7 x 0.3 Mt	9 x 0.3 Mt	13 NEDs x 0.2 Mt
m_{s/c_0} $[kg]$	10754.72	10813.41	10775.73	10819.65	10377.72	10871.90	11170.07
Lowest Mass	73.03	101.95	52.94	76.76	51.14	64.65	41.25
50th percentile	101.91	140.81	76.59	105.34	70.29	88.89	56.77
Highest Mass	134.56	185.82	101.05	139.52	92.70	115.24	74.83

[6] N. Chabot, E. Adams, A. Rivkin, and J. Kalirai, Acta Astronautica, vol. 220, pp. 118– 125, 2024. DOI: https://doi.org/10.1016/j.actaastro.2024.04.001.
[8] M. Vasile and N. Thiry, Advances in Space Research, vol. 57, no. 8, pp. 1805–1819, 2016. DOI: https://doi.org/10.1016/j.asr.2015.11.036.

Single and Multiple Ion Beam Deflection

Multiple pairs of ion thrusters → Number of thruster pairs, N_{pairs}

Multiple IBD spacecraft → Number of spacecraft, $N_{s/c}$

→ **Optimisation variables**

→ **Avoiding inefficient fuel expenditure**

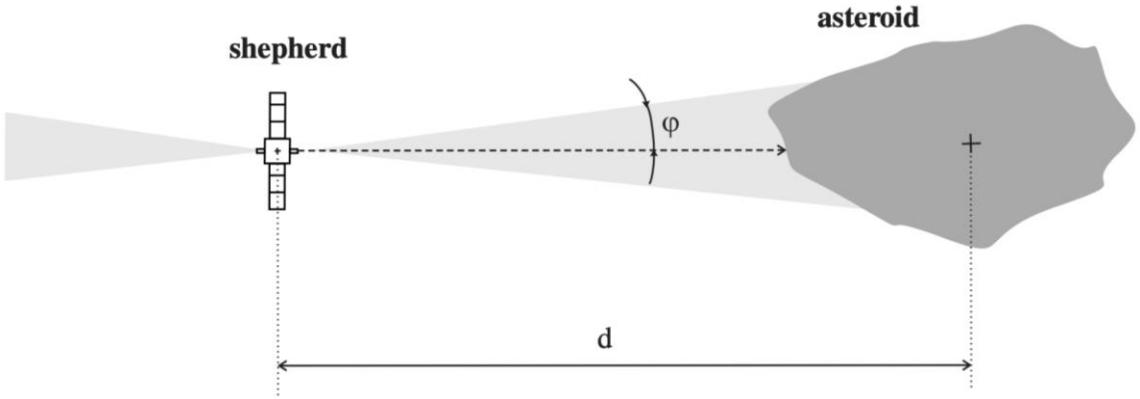

Scheme of IBD spacecraft hovering [9].

Spacecraft gravitational pull on the asteroid

	Early – Launch June 2029			Primary – Launch May 2031			Secondary – Launch June 2033		
	m_{s/c_0} $[kg]$	$N_{s/c}$ $[-]$	δb $[\%\ C]$	m_{s/c_0} $[kg]$	$N_{s/c}$ $[-]$	δb $[\%\ C]$	m_{s/c_0} $[kg]$	$N_{s/c}$ $[-]$	δb $[\%\ C]$
Lowest Mass	12171.07	**1**	**153.75**	10651.21	**1**	**114.00**	11920.59	**3**	**127.82**
50th percentile	12416.02	**1**	**74.26**	10304.53	**2**	**102.69**	10475.57	**4**	**79.32**
Highest Mass	12413.23	**2**	**76.11**	10680.19	**3**	**80.53**	10427.69	**6**	**98.68**
	12176.69	**1**	**36.26**						

[9] C. Bombardelli and J. Peláez, Journal of Guidance, Control, and Dynamics, vol. 34, no. 4, pp. 1270–1272, 2011. DOI: https://doi.org/10.2514/1.51640.

Single and Multiple Laser Ablation

- Continuous irradiation of a small portion of the asteroid surface [10].
- Ablated material forms a **plume of gas and ejecta → Induced thrust.**
- Ablated material **re-condenses on exposed sensitive surfaces [10].**

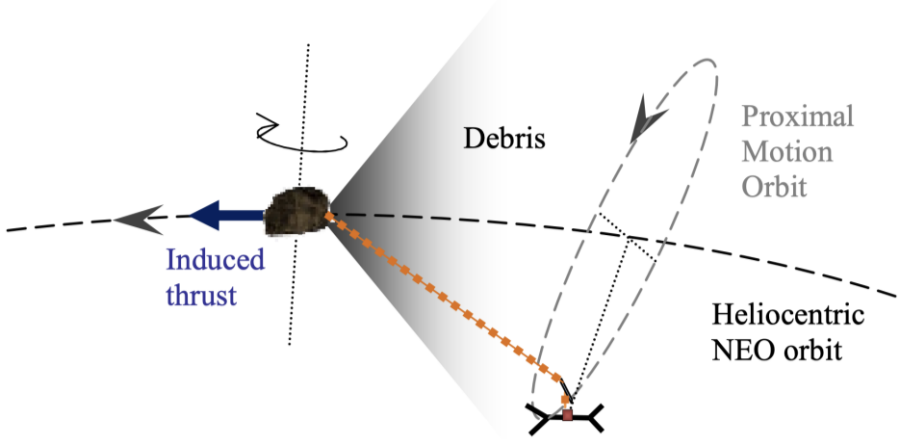

Laser Ablation in formation flight scheme [11].

Optimisation variables

- **SLA →** Hovering distance, d_{hover}
- **Laser input power at 1 AU,** $P_{L,1AU}$
- **MLA →** Spacecraft number, $N_{s/c}$

Spacecraft gravitational pull on the asteroid

	Early – Launch July 2029			Primary – Launch May 2031			Secondary – Launch May 2033		
	$P_{L,1AU}$ $[kW]$	$N_{s/c}$ $[-]$	δb $[\%\ C]$	$P_{L,1AU}$ $[kW]$	$N_{s/c}$ $[-]$	δb $[\%\ C]$	$P_{L,1AU}$ $[kW]$	$N_{s/c}$ $[-]$	δb $[\%\ C]$
Lowest Mass	86.78	**1**	**154.71**	89.26	**1**	**126.43**	88.74	**2**	**133.90**
50th percentile	86.92	**1**	**78.83**	89.56	**2**	**118.21**	89.86	**3**	**99.28**
Highest Mass	87.10	**2**	**89.57**	88.78	**3**	**104.54**	88.50	**4**	**76.16**

[10] M. Vasile, A. Gibbings, I. Watson, and J.-M. Hopkins, Acta Astronautica, vol. 103, pp. 382–394, 2014. DOI: https://doi.org/10.1016/j.actaastro.2014.01.033.
[11] A. Gibbings, J.-M. Hopkins, D. Burns, and M. Vasile, in IAA planetary defense conference, protecting Earth from asteroids: From threat to action, 2011.

Standard and Enhanced Gravity Tractor

- Spacecraft hovers near the asteroid with thrusters angled outward [12].
- **Mutual gravitational attraction** → Small but continous acceleration.

$$a_{GT}(t) = \frac{G\, m_{s/c}(t)}{d_{hover}^2}$$

$$a_{EGT}(t) = \frac{G\,[m_{s/c}(t) + M_{gain}]}{d_{hov,EGT}^2}$$

- **The Enhanced Gravity Tractor (EGT)** collects material from the asteroid surface to increase spacecraft mass [13] → **Close-proximity operations.**

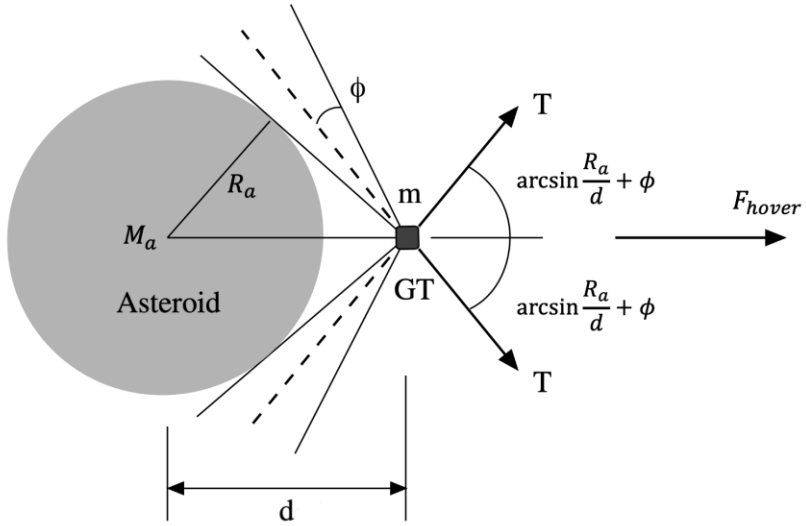

Geometry of gravity tractor hovering [12].

	Early campaign – Launch June 2029				Primary campaign – Launch June 2031			
	Standard GT		Enhanced GT		Standard GT		Enhanced GT	
	d_{hover} $[m]$	δb $[\%\ C]$	$d_{hov,EGT}$ $[m]$	δb $[\%\ C]$	d_{hover} $[m]$	δb $[\%\ C]$	$d_{hov,EGT}$ $[m]$	δb $[\%\ C]$
Lowest Mass	85.74	**51.49**	147.17	**124.32**	85.29	**31.75**	146.74	**80.52**
50th percentile	99.69	**37.40**	196.92	**68.05**	98.99	**22.26**	195.36	**45.51**
Highest Mass	119.95	**24.87**	256.70	**40.70**	122.20	**17.28**	255.07	**26.78**

[12] B. Wie, Journal of guidance, control, and dynamics, vol. 31, no. 5, pp. 1413–1423, 2008. DOI: https://doi.org/10.2514/1.32735.

[13] D.D. Mazanek et al., IAA Planetary Defense Conference, Frascati, Italy, 2015. IAA-PDC-15-04-11. URL: https://ntrs.nasa.gov/citations/20150010968.

CONCLUSION

Key results and TRL considerations

Multiple Kinetic Impactor
- High TRL
- Simple technology
- Strong dependence on physical properties

Launch	$N_{s/c}$ [−]	M_{s/c_0} [kg]	Perihelion	Development time
April – May 2030	**6**	3229	1st November 2032	**Sufficient**

Stand-off NEDs in "Carrier" configuration
- High TRL
- Up to 13 impulses
- Political and legal limitations

Mission	Launch	m_{s/c_0} [kg]	Perihelion	N_{NEDs} [−]
Early	June 2029	10754.72	1st November 2032	**5**
Primary	May 2031	10775.73 − 10819.65	15th December 2034	**5-7**
Secondary	June 2033	10377.72 − 10871.90	27th January 2037	**7-9**
Late	June 2035	11170.07	12th March 2039	**13**

Single and Multiple IBD
- Increasing TRL
- High Performance

Mission	Launch	$N_{s/c}$ [−]	M_{s/c_0} [kg]	Development time
Early	June 2029	**1**	12416.02	**Stringent**
Primary	May 2031	**2-3**	20609.06 − 30913.59	**Sufficient**
Secondary	June 2033	**3-6**	31426.71 − 62853.42	**Extensive**

This project has received funding from the European Research Council (ERC) under the European Union's Horizon Europe research and innovation programme (grant agreement No 101089265 – GREEN SPECIES)

ANALYSIS OF ASTEROID DEFLECTION MISSION OPTIONS FOR THE 2025 PLANETARY DEFENSE CONFERENCE HYPOTHETICAL ASTEROID IMPACT THREAT SCENARIO BY THE ITALIAN SPACE AGENCY DELEGATION AT SMPAG

S. Franzese, E. Basile, E. M. Polli, C. Colombo, P. Vasiliki, M. Castronuovo, J. L. Cano

POLITECNICO MILANO 1863

Planetary Defence Conference 2025 - 6th May 2025

APPENDIX

Appendix – Flyby Reconnaissance Mission Design

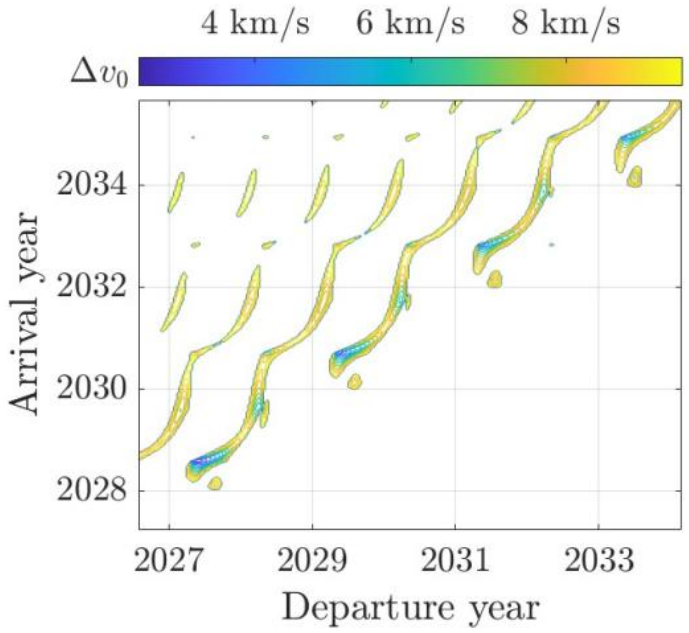

$T_{syn} = 1.89\ years$

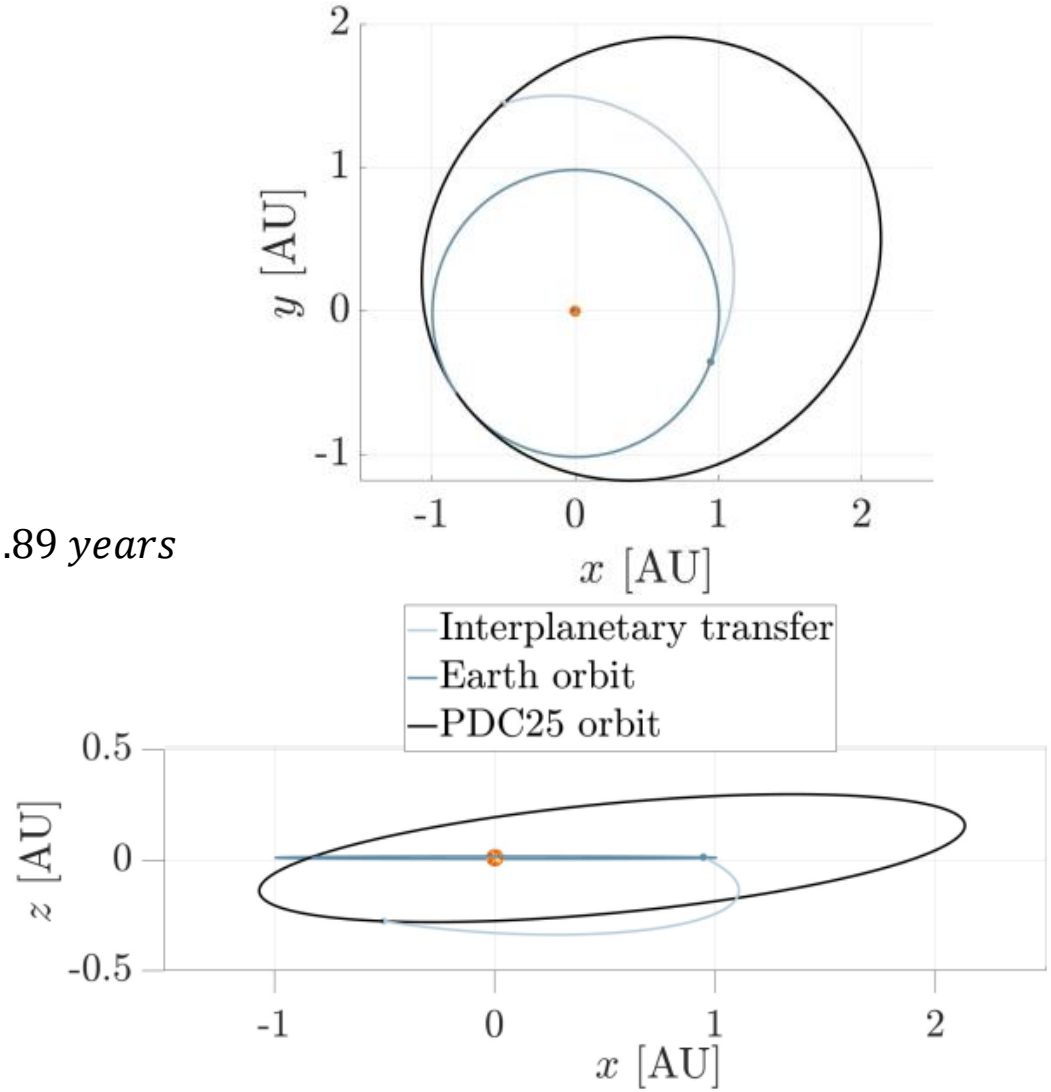

Launch	Arrival	$C_3\ [km^2/s^2]$	Launch Mass $[kg]$	$V_{rel}\ [km/s]$
2027-09-02	2028-03-31	90.80	<1452	10.47

Appendix – MKI model identification

Multiple Kinetic Impactor Model: hypotheses

- Main Assumptions:
  - 1. Two-body problem
  - Gravitational effect of celestial bodies neglected
  - 2. No orbital perturbations
  - 3. Zero nominal miss-distance
  - 4. Time of Minimum Orbit Intersection Distance does not vary

- The assumptions allow for optimal design given the limitations imposed by the computational time
- The model allows for the identification of a nominal solution
- Refinement of the solution can be performed a posteriori

Appendix – MKI model identification

Multiple Kinetic Impactor Model

- **Variation of velocity** due to the individual impact

$$\Delta \boldsymbol{v} = \beta \frac{m_{s/c}}{M_{ast}} \boldsymbol{V}_{rel}$$

- Displacement and velocity variation at **final time**

$$\boldsymbol{\delta r_f} = \boldsymbol{T_{r,v}}\, \Delta \boldsymbol{v} \quad [14]$$

$$\boldsymbol{\delta v_f} = \boldsymbol{T_{v,v}}\, \Delta \boldsymbol{v}$$

- Asteroid's state **update**

$$\boldsymbol{x_f} = \tilde{\boldsymbol{x}}_f + \begin{bmatrix} \boldsymbol{\delta r_f} \\ \boldsymbol{\delta v_f} \end{bmatrix}$$

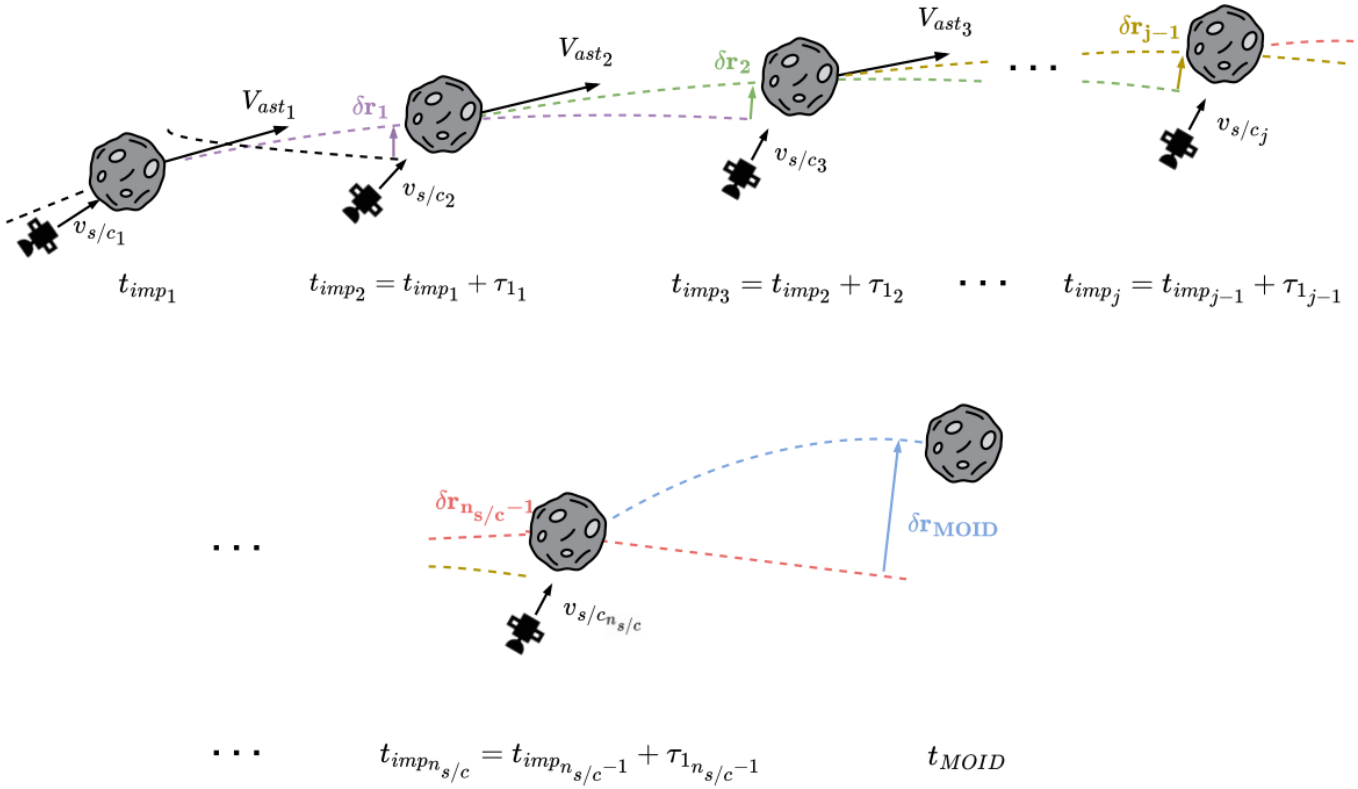

- **Displacement** at Minimum Orbit Intersection Distance

$$\boldsymbol{\delta r_{MOID}} = \boldsymbol{r_{MOID}} - \tilde{\boldsymbol{r}}_{MOID}$$

- Projection of the deflection on the B-plane: **impact parameter**

$$\boldsymbol{b}^* = \mathbf{M}\, \boldsymbol{\delta r_{MOID}} \quad [14]$$

[14] J. L. Gonzalo, C. Colombo, and P. Di Lizia. Journal of Guidance, Control, and Dynamics. URL: https://doi.org/10.2514/1.G005398.

Appendix – MKI model identification

Multiple Kinetic Impactor Model: analytical STM

$$T(\Delta t) = G(t_{imp})G_M(\Delta t)A(t_f) \quad [14]$$

- Variation in the Keplerian elements mapped into a variation in the state of the asteroid at the final time

$$A(t_f) = \begin{bmatrix} A_r(t_f) \\ A_v(t_f) \end{bmatrix}$$

$$A_r(t_f) = \begin{bmatrix} \frac{R}{a} & -a\cos\theta_f & 0 & 0 & 0 & \frac{ae\sin\theta_f}{\sqrt{1-e^2}} \\ 0 & \frac{R\sin\theta_f(2+e\cos\theta_f)}{1-e^2} & 0 & R\cos i & R & \frac{R(1+e\cos\theta_f)^2}{(1-e^2)^{3/2}} \\ 0 & 0 & R\sin(\omega+\theta_f) & -R\cos(\omega+\theta_f)\sin i & 0 & 0 \end{bmatrix}$$

$$A_v(t_f) = \begin{bmatrix} -\frac{eH\sin f}{2ap} & -\frac{H\sin f}{(1-e^2)R} & 0 & -\frac{H\cos i}{R} & -\frac{H}{R} & -\frac{aH}{\sqrt{1-e^2R^2}} \\ -\frac{H}{2aR} & \frac{H(e+\cos f)}{(1-e^2)p} & 0 & \frac{eH\cos i\sin f}{p} & \frac{eH\sin f}{p} & 0 \\ 0 & 0 & \frac{H(e\cos\omega+\cos(\omega+f))}{p} & \frac{H\sin i(e\sin\omega+\sin(\omega+f))}{p} & 0 & 0 \end{bmatrix}$$

[14] J. L. Gonzalo, C. Colombo, and P. Di Lizia. Journal of Guidance, Control, and Dynamics. URL: https://doi.org/10.2514/1.G005398.

Appendix – MKI model identification

Multiple Kinetic Impactor Model: analytical STM

$$T(\Delta t) = G(t_{imp}) G_M(\Delta t) A(t_f) \quad [14]$$

- Change in orbital parameters during the propagation time (variation in the asteroid's mean anomaly due to a variation in the semi-major axis)

$$G_M(\Delta t) = \begin{bmatrix} 1 & 0 & 0 & 0 & 0 & 0 \\ 0 & 1 & 0 & 0 & 0 & 0 \\ 0 & 0 & 1 & 0 & 0 & 0 \\ 0 & 0 & 0 & 1 & 0 & 0 \\ 0 & 0 & 0 & 0 & 1 & 0 \\ -\frac{3\sqrt{\mu_S}\Delta t}{2a^{\frac{5}{2}}} & 0 & 0 & 0 & 0 & 1 \end{bmatrix}$$

[14] J. L. Gonzalo, C. Colombo, and P. Di Lizia. Journal of Guidance, Control, and Dynamics. URL: https://doi.org/10.2514/1.G005398.

Appendix – MKI model identification

Multiple Kinetic Impactor Model: analytical STM

$$T(\Delta t) = G(t_{imp})G_M(\Delta t)A(t_f) \quad [14]$$

- Change in orbital parameters during the propagation time (variation in the asteroid's mean anomaly due to a variation in the semi-major axis)

$$G(t_{imp}) = \begin{bmatrix} G_r(t_{imp}) & G_v(t_{imp}) \end{bmatrix}$$

$$G_r(t_{\text{imp}}) = \begin{bmatrix} G_{r_{11}} & G_{r_{12}} & 0 \\ G_{r_{21}} & G_{r_{22}} & 0 \\ 0 & 0 & G_{r_{33}} \\ 0 & 0 & G_{r_{43}} \\ G_{r_{51}} & G_{r_{52}} & G_{r_{53}} \\ G_{r_{61}} & G_{r_{62}} & 0 \end{bmatrix}$$

$$G_{r_{11}} = \frac{2a^2 R_t}{R_{\text{imp}}^3} \qquad G_{r_{12}} = \frac{2a^2 R_n}{R_{\text{imp}}^3} \qquad G_{r_{21}} = \left(\frac{H^2 a}{R_{\text{imp}}^3} - V_{\text{imp}}^2\right)\frac{R_t}{\mu_S a e} + \frac{R_{\text{imp}} \sin\theta_{\text{imp}} V_{\text{imp}}}{aH}$$

$$G_{r_{22}} = \left(\frac{H^2 a}{R_{\text{imp}}^3} - V_{\text{imp}}^2\right)\frac{R_n}{\mu_S a e} \qquad G_{r_{33}} = \frac{\sin(\omega + \theta_{\text{imp}}) + e\sin\omega}{p} \qquad G_{r_{43}} = \frac{-(\cos(\omega + \theta_{\text{imp}}) + e\cos\omega)}{p\sin i}$$

$$G_{r_{51}} = \frac{R_{\text{imp}} \sin\theta_{\text{imp}} \left[(p + R_{\text{imp}})\frac{V_{\text{imp}}^2}{R_{\text{imp}}^2} - H^2\frac{(p+e^2 R_{\text{imp}})}{pR_{\text{imp}}^3}\right]}{eH^2} R_t - \frac{R_{\text{imp}} V_{\text{imp}} (\cos\theta_{\text{imp}} + e)}{Hep}$$

$$G_{r_{52}} = \frac{R_{\text{imp}} \sin\theta_{\text{imp}} \left[(p + R_{\text{imp}})\frac{V_{\text{imp}}^2}{R_{\text{imp}}^2} - H^2\frac{(p+e^2 R_{\text{imp}})}{pR_{\text{imp}}^3}\right]}{eH^2} R_n \qquad G_{r_{53}} = \frac{\cos i(\cos(\omega + \theta_{\text{imp}}) + e\cos\omega)}{p\sin i}$$

$$G_{r_{61}} = \frac{b\left[R_{\text{imp}}^2 - a(p + R_{\text{imp}})\right]\sin\theta_{\text{imp}}}{a^2 epR_{\text{imp}}^2} R_t + \frac{\cos\theta_{\text{imp}} R_{\text{imp}} V_{\text{imp}} b}{Ha^2 e}$$

$$G_{r_{62}} = \frac{b\left[R_{\text{imp}}^2 - a(p + R_{\text{imp}})\right]\sin\theta_{\text{imp}}}{a^2 epR_{\text{imp}}^2} R_n$$

[14] J. L. Gonzalo, C. Colombo, and P. Di Lizia. Journal of Guidance, Control, and Dynamics. URL: https://doi.org/10.2514/1.G005398.

Appendix – MKI model identification

Multiple Kinetic Impactor Model: analytical STM

$$T(\Delta t) = G(t_{imp})G_M(\Delta t)A(t_f) \quad [14]$$

- Change in orbital parameters during the propagation time (variation in the asteroid's mean anomaly due to a variation in the semi-major axis)

$$G(t_{imp}) = \begin{bmatrix} G_r(t_{imp}) & G_v(t_{imp}) \end{bmatrix}$$

$$G_v(t_{imp}) = \begin{bmatrix} \frac{2a^2 V_{\text{imp}}}{\mu_S} & 0 & 0 \\ \frac{2(e+\cos\theta_{\text{imp}})}{V_{\text{imp}}} & \frac{-R_{\text{imp}}\sin\theta_{\text{imp}}}{aV_{\text{imp}}} & 0 \\ 0 & 0 & \frac{R_{\text{imp}}\cos(\omega+\theta_{\text{imp}})}{H} \\ 0 & 0 & \frac{R_{\text{imp}}\sin(\omega+\theta_{\text{imp}})}{H\sin i} \\ \frac{2\sin\theta_{\text{imp}}}{eV_{\text{imp}}} & \frac{2e+\frac{R_{\text{imp}}}{a}\cos\theta_{\text{imp}}}{eV_{\text{imp}}} & \frac{-R_{\text{imp}}\sin(\omega+\theta_{\text{imp}})\cos i}{H\sin i} \\ \frac{-2b\sin\theta_{\text{imp}}(1+e^2\frac{R_{\text{imp}}}{p})}{eaV_{\text{imp}}} & \frac{-bR_{\text{imp}}\cos\theta_{\text{imp}}}{ea^2V_{\text{imp}}} & 0 \end{bmatrix}$$

[14] J. L. Gonzalo, C. Colombo, and P. Di Lizia. Journal of Guidance, Control, and Dynamics. URL: https://doi.org/10.2514/1.G005398.

Appendix – MKI optimisation strategy

Hypotheses and variables

HYPOTHESIS

- **Launcher**: **Falcon 9 Heavy** (Expendable)

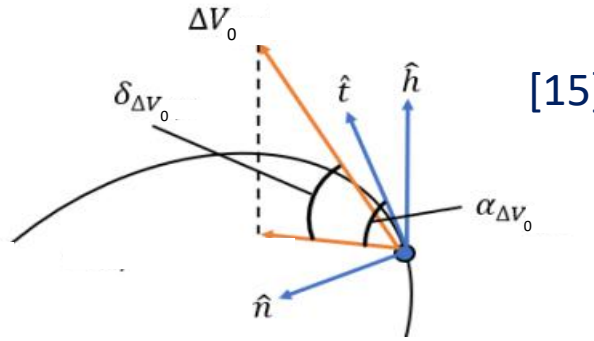

[15]

- **Launch date**: earliest **June 2029**

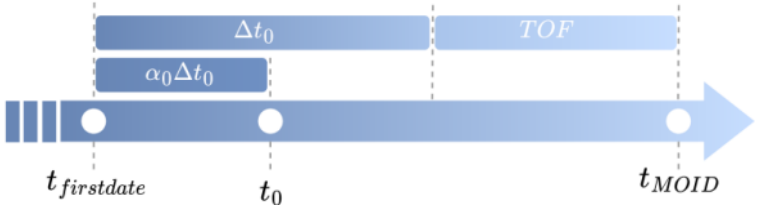

- **Interplanetary trajectory**: two arcs divided by a **Deep Space Manoeuvre**

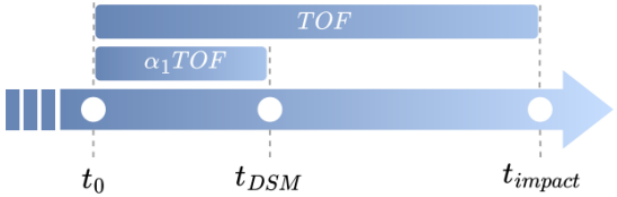

OPTIMISATION VARIABLES INVOLVED [15]

Involved in optimisation	Variables	Nomenclature
Launch mass	Mass	m_{s/c_0}
Launch specific energy	Variation of velocity	Δv_0
Launch angles	In-plane angle	$\alpha_{\Delta v_0}$
	Out-of-plane angle	$\delta_{\Delta v_0}$

Involved in optimisation	Variables	Nomenclature
Departure date	Departure coefficient	α_0

Involved in optimisation	Variables	Nomenclature
Total Time of Flight	Time of Flight	TOF
DSM position	DSM coefficient	α_1
Number of Lambert revolutions	#	N_{rev}

[15] Adapted from: I. Bolzoni. Master's thesis, Politecnico di Milano, 2021. URL: https://www.politesi.polimi.it/handle/10589/182100.

Appendix – MKI optimisation strategy

Hypotheses and variables

HYPOTHESIS

- **Launcher**: **Falcon 9 Heavy** (Expendable)

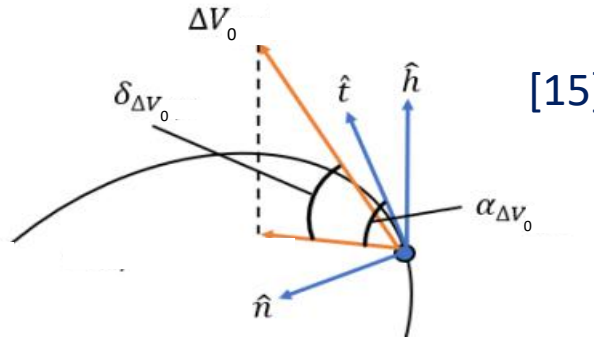

[15]

- **Launch date**: separation between launches

- **Interplanetary trajectory**: two arcs divided by a **Deep Space Manoeuvre**, separation between launches

OPTIMISATION VARIABLES INVOLVED [15]

Involved in optimisation	Variables	Nomenclature
Launch mass	Mass	m_{s/c_0}
Launch specific energy	Variation of velocity	Δv_0
Launch angles	In-plane angle	$\alpha_{\Delta v_0}$
	Out-of-plane angle	$\delta_{\Delta v_0}$

Involved in optimisation	Variables	Nomenclature
Interval between launches	Separation	τ_0

Involved in optimisation	Variables	Nomenclature
Interval between impacts	Separation	τ_1
DSM position	DSM coefficient	α_1
Number of Lambert revolutions	#	N_{rev}

[15] Adapted from: I. Bolzoni. Master's thesis, Politecnico di Milano, 2021. URL: https://www.politesi.polimi.it/handle/10589/182100.

Appendix – MKI optimisation strategy

Bounds and constraints

- Optimization variables are **bounded** → bounds are selected through an **iterative process**

1st Spacecraft

Variable	α_0	α_1	TOF	Δv_0	$\alpha_{\Delta v_0}$	$\delta_{\Delta v_0}$	m_{s/c_0}	N_{rev}
Lower Bound	0	0.3	800 days	2 km/s	0	0	100 kg	1
Upper Bound	0.4	0.6	1000 days	5.5 km/s	2π	$\pi/2$	2000 kg	1

Nth Successive Spacecraft

Variable	τ_0	τ_1	α_1	Δv_0	$\alpha_{\Delta v_0}$	$\delta_{\Delta v_0}$	m_{s/c_0}	N_{rev}
Lower Bound	**10 days**	**14 days** [6]	0.3	2 km/s	0	0	100 kg	1
Upper Bound	21 days	21 days	0.6	5.5 km/s	2π	$\pi/2$	2000 kg	1

- Optimization problem is **constrained** → two constraints for each spacecraft are selected from **analysis** and **literature**

	Aim	Formulation	Value
1st Constraint	Spacecraft design	$m_{s/c} \geq p\, m_{s/c_0}$	p= 30% [16]
2nd Constraint	Fragmentation avoidance	$\Delta v \leq f\, v_{esc}$	f= 10% [17]

[6] N. Chabot, E. Adams, A. Rivkin, and J. Kalirai, Acta Astronautica, vol. 220, pp. 118– 125, 2024. URL: https://doi.org/10.1016/j.actaastro.2024.04.001.
[16] J. R. Wertz, D. F. Everett, and J. J. Puschell. Space mission engineering: the new SMAD. 2011.
[17] P. Michel, W. Benz, and D. C. Richardson. Planetary and Space Science, 2004. URL: https://doi.org/10.1016/j.pss.2004.07.008.

Appendix – MKI nominal mission

Three-spacecraft mission

- **Three spacecraft** are sufficient for ensuring the minimum **southwards impact parameter** requirement

Spacecraft	Launch	DSM	Arrival	c_3 $[km^2/s^2]$	m_{s/c_0} [kg]	$m_{s/c}$ [kg]	V_{rel} [km/s]	b^* [km]	Δv
#1	**2030-04-28**	2031-04-24	2032-10-05	12.45	1041	713	9.58	5696	6.87 % v_{esc}
#2	2030-05-10	2031-05-04	2032-10-22	10.91	1179	1126	8.47	14578	9.58 % v_{esc}
#3	2030-05-21	2031-05-20	**2032-11-07**	10.70	1141	794	8.45	20955	6.74 % v_{esc}

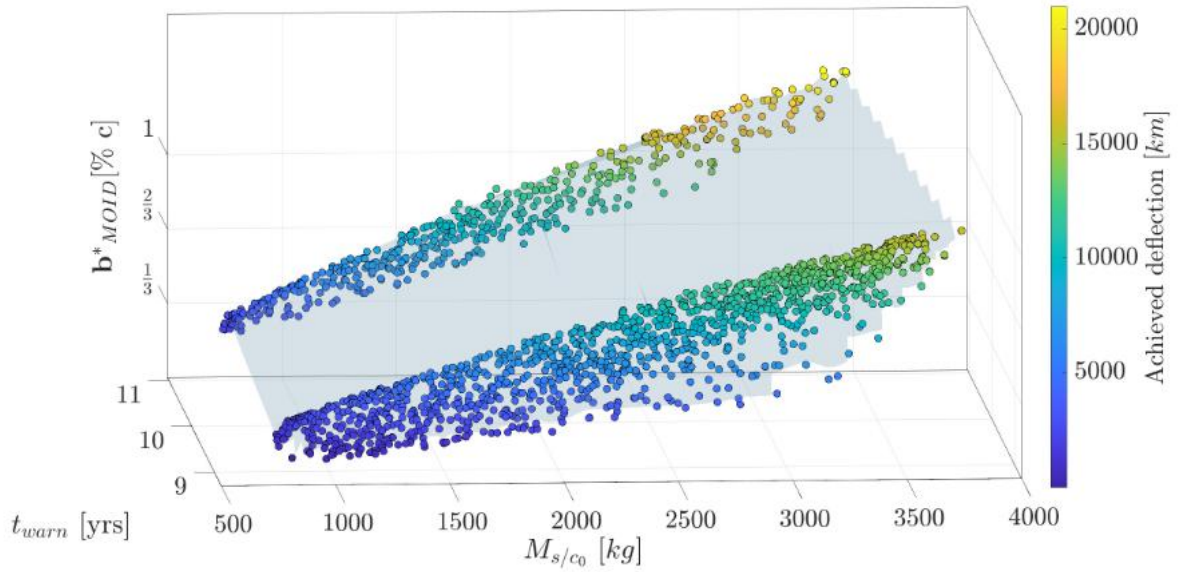

Pareto-optimal set of solutions

Minimum impact parameter requirement: b^*_{south} = ***15352 km***

Fragmentation avoidance requirement: $\Delta v \leq 10\%\ v_{esc}$

- Obtained solution has **36.5% margin** over the requirement
- Requirement Compliant ✓

Appendix – MKI: Sensitivity Analysis

Monte Carlo simulations

Uncertainty Source	Variables involved	Number of samples
Asteroid's Position	Asteroid position at first impact ($\boldsymbol{r_{imp}}$)	100'000
Relative Navigation Error	Relative velocity at impacts ($\boldsymbol{V_{rel}}$)	200
	Relative position at impact ($\boldsymbol{r_c}$)	1000
Physical Parameters	Asteroid's mass ($\boldsymbol{M_{ast}}$)	5000
	Momentum enhancement factor (β)	200

- The resulting velocity change from one sample of the population is propagated **deterministically**
- Effects of different **uncertainty sources** are **decoupled**
  - At least **95.45%** of the samples satisfy the mission requirements
  - Requirements are satisfied with **2σ confidence level**

} Mission is **ROBUST** to perturbations

MKI: Sensitivity Analysis

Asteroid's position

DATA

- Covariance matrix exploited for the generation of samples:

$$P_0 = \begin{bmatrix} 53.50 & -167.62 & -57.00 \\ -167.62 & 662.62 & 161.36 \\ -57.00 & 161.36 & 93.90 \end{bmatrix} km^2 \quad [18]$$

RESULTS

- All solutions **compliant** with the **minimum impact parameter** requirement
- All solutions **compliant** with the **fragmentation avoidance** requirement

Minimum impact parameter requirement: b^*_{south} = ***15352 km***

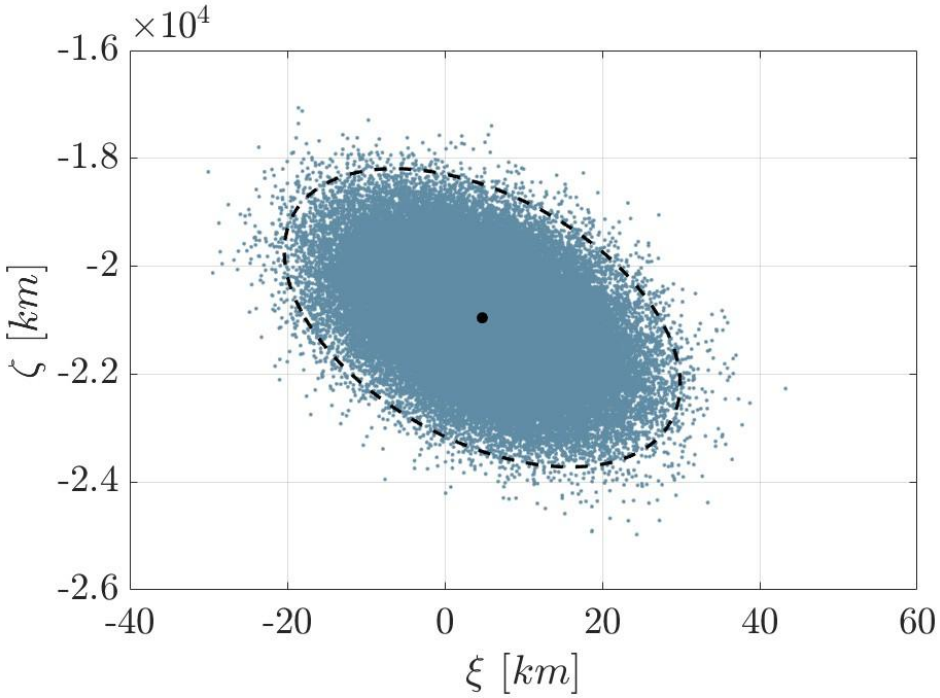

Impact parameter variation with position uncertainty.

[18] By courtesy of D. Farnocchia during internal SMPAG discussion.

MKI: Sensitivity Analysis

Relative velocity

DATA

- Covariance matrix exploited for the generation of samples: $P_{nav} = \begin{bmatrix} 100^2 & 0 & 0 \\ 0 & 100^2 & 0 \\ 0 & 0 & 100^2 \end{bmatrix} \frac{m^2}{s^2}$ [19]

RESULTS

- All solutions **compliant** with the requirements

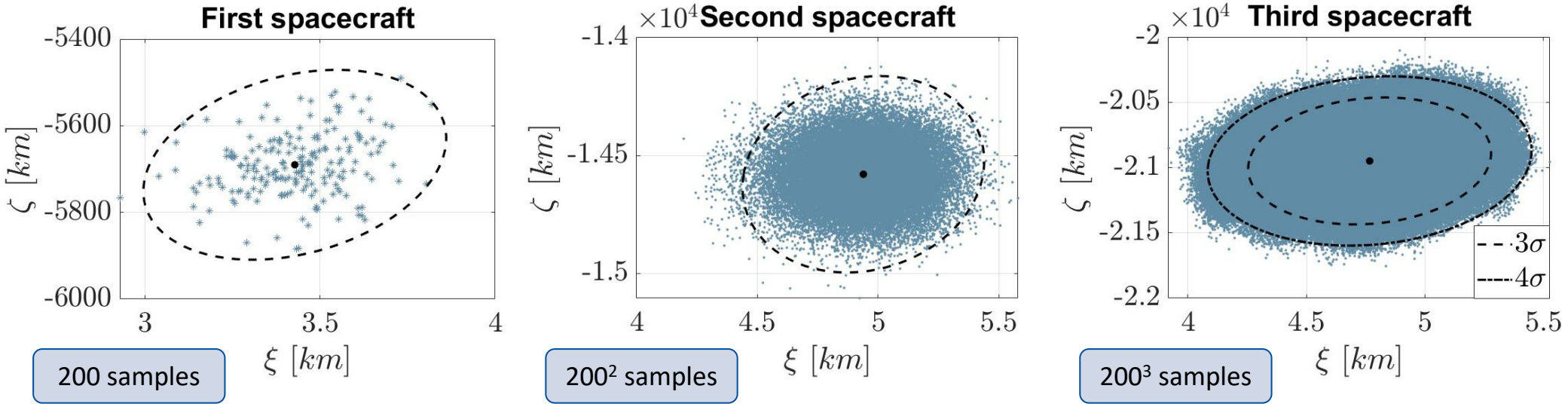

Impact parameter variation with uncertainty on relative velocity.

[19] A. F. Cheng, A. S. Rivkin, P. Michel, J. Atchison, O. Barnouin, L. Benner, N. L. Chabot, C. Ernst, E. G. Fahnestock, M. Kuep-pers, et al. Planetary and Space Science157, 2018. URL: https://doi.org/10.1016/j.pss.2018.02.015.

Appendix – MKI: Sensitivity Analysis

Impact location on asteroid's surface

DATA

a_{ast}	b_{ast}	c_{ast}	T_{ast}	α_{spin}	δ_{spin}
59.5 m	122 m	58.5 m	3 hours	253 °	74 °

Ellipsoidal coordinates

ϑ_r polar angle $[0,\ \pi]$

ϕ_r azimuthal angle $[0,\ 2\pi]$

METHOD

- Linear momentum conservation $m_{s/c}\boldsymbol{V}_{rel} = M_{ast}\,\Delta\boldsymbol{v} + \boldsymbol{P}_{ejecta}$
- Net ejecta momentum $\boldsymbol{P}_{ejecta} = (1-\beta)\ m_{s/c}\,\boldsymbol{V}_{rel} + m_{ejecta}\,\boldsymbol{\omega}_{ast} \times \boldsymbol{r}_{crater}$ [20]

$$\boldsymbol{r}_{crater} = \begin{bmatrix} a_{ast}\sin\vartheta_r\cos\phi_r \\ b_{ast}\sin\vartheta_r\sin\phi_r \\ c_{ast}\cos\vartheta_r \end{bmatrix}$$

RESULTS

- The solution is expected to perform **robustly** to cratering location variations

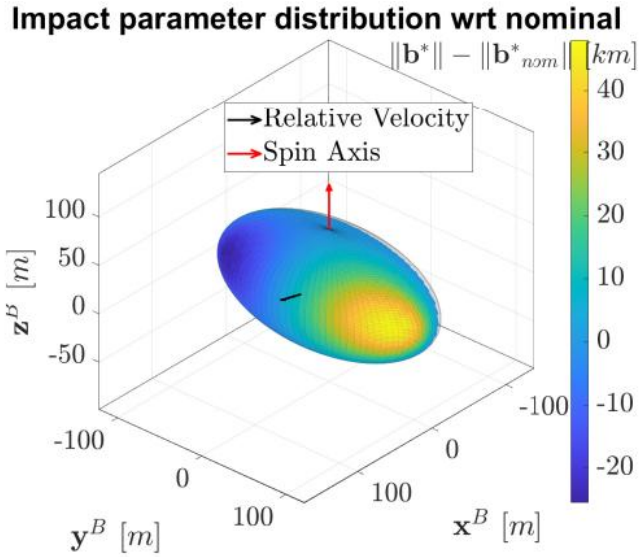

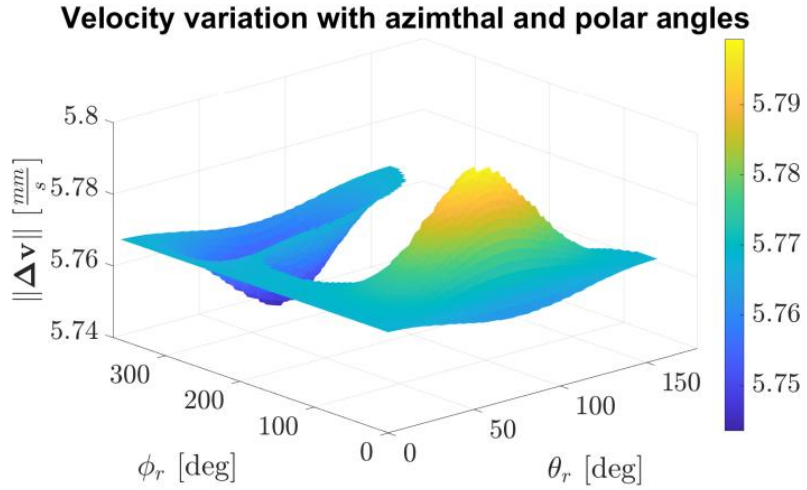

[20] F. Zhang, B. Xu, C. Circi, and L. Zhang. Advances in Space Research, 2017. URL: https://doi.org/10.1016/j.asr.2017.01.003.

Appendix – MKI robust mission design

Bounds' modification

- Updated **fragmentation requirement** $\Delta v \leq 4\%\, v_{escape}$

- Given the increasing number of spacecraft (**increasing duration** for the MKI campaign to be completed), bounds modifications is required

1st Spacecraft

Variable	α_0	α_1	TOF	Δv_0	$\alpha_{\Delta v_0}$	$\delta_{\Delta v_0}$	m_{s/c_0}	N_{rev}
Lower Bound	**0.07**	0.3	**870 days**	3 km/s	0	0	100 kg	1
Upper Bound	**0.13**	0.6	**930 days**	5 km/s	2π	$\pi/2$	**900 kg**	1

Nth Successive Spacecraft

Variable	τ_0	τ_1	α_1	Δv_0	$\alpha_{\Delta v_0}$	$\delta_{\Delta v_0}$	m_{s/c_0}	N_{rev}
Lower Bound	**3 days**	**14 days**	0.3	3 km/s	0	0	100 kg	1
Upper Bound	**10 days**	**17 days**	0.6	5 km/s	2π	$\pi/2$	**900 kg**	1

Appendix – Nominal three-spacecraft mission

STM propagation compared to Cartesian propagation

Spacecraft	Launch	DSM	Arrival	c_3	m_{s/c_0}	$m_{s/c}$	V_{rel}	b^*	Δv
#1	2030-04-28	2031-04-24	2032-10-05	12.45 km²/s²	1041 kg	713 kg	9.58 km/s	5696 km	6.87 % v_{esc}
#2	2030-05-10	2031-05-04	2032-10-22	10.91 km²/s²	1179 kg	1126 kg	8.47 km/s	14578 km	9.58 % v_{esc}
#3	2030-05-21	2031-05-20	2032-11-07	10.70 km²/s²	1141 kg	794 kg	8.45 km/s	20955 km	6.74 % v_{esc}

Spacecraft	Launch	DSM	Arrival	c_3	m_{s/c_0}	$m_{s/c}$	V_{rel}	b^*	Δv
#1	2030-04-28	2031-04-24	2032-10-05	12.45 km²/s²	1041 kg	713 kg	9.58 km/s	**5697 km**	6.87 % v_{esc}
#2	2030-05-10	2031-05-04	2032-10-22	10.91 km²/s²	1179 kg	1126 kg	8.47 km/s	**14579 km**	9.58 % v_{esc}
#3	2030-05-21	2031-05-20	2032-11-07	10.70 km²/s²	1141 kg	794 kg	8.45 km/s	**20956 km**	6.74 % v_{esc}

Appendix – Cartesian optimisation

Maximum impact parameter: Cartesian

Spacecraft	Launch	DSM	Arrival	c_3	m_{s/c_0}	$m_{s/c}$	V_{rel}	b^*	Δv
#1	2030-04-30	2031-05-07	2032-10-02	14.24 km^2/s^2	1263 kg	891 kg	10.47 km/s	7302 km	9.36 % v_{esc}
#2	2030-05-21	2031-05-20	2032-10-20	9.58 km^2/s^2	1178 kg	1088 kg	9.12 km/s	15996 km	9.97 % v_{esc}
#3	2030-06-06	2031-05-29	2032-11-06	8.30 km^2/s^2	1535 kg	998 kg	8.50 km/s	23917 km	8.52 % v_{esc}

Maximum impact parameter: STM

Spacecraft	Launch	DSM	Arrival	c_3	m_{s/c_0}	$m_{s/c}$	V_{rel}	b^*	Δv
#1	2030-05-18	2031-05-03	2032-10-01	16.69 km^2/s^2	1177 kg	874 kg	10.81 km/s	7230 km	9.48 % v_{esc}
#2	2030-06-01	2031-05-25	2032-10-19	13.27 km^2/s^2	1069 kg	1025 kg	9.70 km/s	15696 km	9.98 % v_{esc}
#3	2030-06-16	2031-06-02	2032-11-05	12.49 km^2/s^2	1281 kg	824 kg	9.05 km/s	23488 km	7.49 % v_{esc}

Appendix – Shape-based low-thrust trajectory

- **Equation of motion** of a spacecraft in the **heliocentric inertial reference frame** → $\ddot{\boldsymbol{r}}_{s/c} + \frac{\mu_S}{r_{s/c}} \boldsymbol{r}_{s/c} = \boldsymbol{T}_a$

- **Spacecraft heliocentric position vector, $\boldsymbol{r}_{s/c}$**, shaped as a **function of initial and target orbital elements** using Fourier series with coefficients obtained imposing the boundary constraints [21] → $\boldsymbol{r}_{s/c}(\theta) = \Phi_1(\theta)\,\boldsymbol{r}_1 + \Phi_2(\theta)\,\boldsymbol{r}_2$

- Shaping vectors $\boldsymbol{r}_1$ and $\boldsymbol{r}_2$ → $$\boldsymbol{r}_k = a_k \frac{(1-e_k^2)}{1+e_k\cos\theta_k}\cos\theta_k\,\boldsymbol{p}_k + a_k \frac{(1-e_k^2)}{1+e_k\cos\theta_k}\sin\theta_k\,\boldsymbol{q}_k \quad \text{with: } k = 1,2$$

- Direction vectors $\boldsymbol{p}_k$ and $\boldsymbol{q}_k$ → $$\boldsymbol{p}_k = \begin{bmatrix} \cos\omega_k\cos\Omega_k - \sin\omega_k\sin\Omega_k\cos i_k \\ \cos\omega_k\sin\Omega_k + \sin\omega_k\cos\Omega_k\cos i_k \\ \sin\omega_k\sin i_k \end{bmatrix}; \quad \boldsymbol{q}_k = \begin{bmatrix} -\sin\omega_k\cos\Omega_k - \cos\omega_k\sin\Omega_k\cos i_k \\ -\sin\omega_k\sin\Omega_k + \cos\omega_k\cos\Omega_k\cos i_k \\ \cos\omega_k\sin i_k \end{bmatrix}$$

- **The only variables are the true anomalies** → $\theta_1 = \theta_{10} + f$ and $\theta_2 = \theta_{20} + f$
  - θ_{10} → True anomaly of the spacecraft at departure point [21];
  - θ_{20} → Virtual true anomaly of the target orbit at initial time [21];
  - f → Unwrapped true anomaly of the transfer orbit [21].

Total unwrapped transfer angle

$$f_{end} = \theta_{arr} - \theta_{20} + 2\pi\,N_{rev}$$

[21] K. Zeng, Y. Geng, and B. Wu, Aerospace Science and Technology, vol. 62, pp. 87–97, 2017. DOI: https://doi.org/10.1016/j.ast.2016.12.006.

Appendix – Shape-based low-thrust trajectory

- $\boldsymbol{r}_{s/c}$ is parametrised by θ → To obtain $\ddot{\boldsymbol{r}}_{s/c}$, the expression of $\dot{\theta}$ is derived first [21].
- Let $\boldsymbol{h}_1$ and $\boldsymbol{h}_2$ be the angular momentum vectors of the initial and target orbits, respectively → The change of the spacecraft angular momentum:

$$h = \left\|\boldsymbol{r}_{s/c} \times \dot{\boldsymbol{r}}_{s/c}\right\| = \left\|\boldsymbol{r}_{s/c} \times \frac{\partial \boldsymbol{r}_{s/c}}{\partial \theta}\right\| \dot{\theta} = \Phi_1 h_1 + \Phi_2 h_2 \implies \dot{\theta} = \frac{\Phi_1 h_1 + \Phi_2 h_2}{\left\|\boldsymbol{r}_{s/c} \times \frac{\partial \boldsymbol{r}_{s/c}}{\partial \theta}\right\|}$$

- Using $\dot{\theta}$, the derivatives $\dot{\boldsymbol{r}}_{s/c}$ and $\ddot{\boldsymbol{r}}_{s/c}$ are obtained [21] → From the equation of motion, the spacecraft low-thrust acceleration $\boldsymbol{T}_a(\theta)$ is retrieved, and integrated over $[0, f_{end}]$ to obtain the Δv_{SB} for the shape-based low-thrust trajecrory.

$$\boldsymbol{T}_a(\theta) = \ddot{\boldsymbol{r}}_{s/c} + \frac{\mu_S}{r_{s/c}} \boldsymbol{r}_{s/c} \rightarrow \Delta v_{SB} = \int_0^{f_{end}} \frac{\|\boldsymbol{T}_a(\theta)\|}{\dot{\theta}} \rightarrow m_{s/c_{arr}} = m_{s/c_0} \exp\left(-\frac{\Delta v_{SB} \times 10^3}{I_{sp}\, g_0}\right)$$

Shape-based low-thrust trajectory Time of Flight

$$\mathrm{ToF_{SB}} = \int_0^{f_{end}} \frac{1}{\dot{\theta}}\, d\theta = \int_0^{f_{end}} \left\|\boldsymbol{r}_{s/c} \times \frac{\partial \boldsymbol{r}_{s/c}}{\partial \theta}\right\| \frac{1}{\Phi_1 h_1 + \Phi_2 h_2}\, \mathrm{d}\theta$$

Fuel mass

$$m_{f_{SB}} = m_{s/c_0} - m_{s/c_{arr}}$$

[21] K. Zeng, Y. Geng, and B. Wu, Aerospace Science and Technology, vol. 62, pp. 87–97, 2017. DOI: https://doi.org/10.1016/j.ast.2016.12.006.

Appendix – Time-optimal low-thrust trajectory

- Spacecraft affected by the Sun gravitational acceleration, and the acceleration due to the on-board propulsion system [22].
- Spacecraft dynamic equations in the 3D Heliocentric Two-Body Problem → **7-dimensional state vector:** $\boldsymbol{s} = \left[\boldsymbol{r}_{s/c} \;\; \boldsymbol{v}_{s/c} \;\; m_{s/c}\right]^T$.
- **The vector of co-states** → $\boldsymbol{\lambda} = [\,\boldsymbol{\lambda}_r \;\; \boldsymbol{\lambda}_v \;\; \lambda_m]^T$.

$$\dot{\boldsymbol{s}} = \boldsymbol{f}(\boldsymbol{s}, u) = \begin{cases} \dot{\boldsymbol{r}}_{s/c} = \boldsymbol{v}_{s/c} \\ \dot{\boldsymbol{v}}_{s/c} = -\dfrac{\mu_S}{r_{s/c}^3}\,\boldsymbol{r}_{s/c} + u\,\dfrac{T_{max}}{m_{s/c}}\,\hat{\boldsymbol{\alpha}} \\ \dot{m}_{s/c} = -u\,\dfrac{T_{max}}{I_{sp} g_0} \end{cases}$$

- **Hamiltonian for the time-optimal problem [22]:**

$$H(\boldsymbol{s}, \boldsymbol{\lambda}, \boldsymbol{u}) = l(\boldsymbol{s}, \boldsymbol{u}, t) + \boldsymbol{\lambda} \cdot \boldsymbol{f}(\boldsymbol{s}, u) = 1 + \begin{bmatrix} \boldsymbol{\lambda}_r \\ \boldsymbol{\lambda}_v \\ \lambda_m \end{bmatrix} \cdot \begin{bmatrix} \boldsymbol{v}_{s/c} \\ -\dfrac{\mu_S}{r_{s/c}^3}\,\boldsymbol{r}_{s/c} + u\,\dfrac{T_{max}}{m_{s/c}}\,\hat{\boldsymbol{\alpha}} \\ -u\,\dfrac{T_{max}}{I_{sp} g_0} \end{bmatrix}$$

Objective function in Lagrange form [22]

$$J = \int_{t_0}^{t_{arr}} l(\boldsymbol{s}, \boldsymbol{u}, t)\, dt = \int_{t_0}^{t_{arr}} dt = \text{ToF}$$

Co-states dynamics using Euler-Lagrange equations by means of Hamiltonian [23]

$$\dot{\boldsymbol{\lambda}} = -\left[\frac{\partial H}{\partial \boldsymbol{s}}\right]^T = \begin{cases} \dot{\boldsymbol{\lambda}}_r = -\left[\dfrac{\partial H}{\partial \boldsymbol{r}_{s/c}}\right]^T \\ \dot{\boldsymbol{\lambda}}_v = -\left[\dfrac{\partial H}{\partial \boldsymbol{v}_{s/c}}\right]^T \\ \dot{\lambda}_m = -\dfrac{\partial H}{\partial m_{s/c}} \end{cases}$$

[22] E. Taheri, N. I. Li, and I. Kolmanovsky, in 2016 American Control Conference (ACC), pp. 4053–4058, IEEE, 2016. DOI: https://doi.org/10.1109/ACC. 2016.7525558.
[23] A. Ioffe, Transactions of the american mathematical society, vol. 349, no. 7, pp. 2871–2900, 1997. DOI: https://doi.org/10.1090/S0002-9947-97-01795-9.

Appendix – Time-optimal low-thrust trajectory

- **Unknown arrival time** → Target is locus of points describing the NEO heliocentric orbit [25]: $\boldsymbol{\psi}(t_{arr}) = [\boldsymbol{r}(t_{arr}),\ \boldsymbol{v}(t_{arr})]^T$.
- **Unknown fuel required** → Final mass of the spacecraft left free [25] → The associated co-state at final time: $\lambda_m(t_{arr}) = 0$.

- **Boundary conditions** →

$$\begin{cases} \boldsymbol{s}(t_0) = [\boldsymbol{r}_E(t_0), \boldsymbol{v}_E + \Delta \boldsymbol{V}_{s/c}, m_{s/c_0}]^T \\ \boldsymbol{s}^*(t_{arr}) = \boldsymbol{\psi}(t_{arr});\ \lambda_m(t_f) = 0 \end{cases}$$

Conditions on control variables u and $\hat{\boldsymbol{\alpha}}$ **using PMP [24]**

$$\boldsymbol{u} = \arg\min_{\boldsymbol{u} \in U} H(\boldsymbol{s}, \boldsymbol{\lambda}, \boldsymbol{u})$$

Where: $U = \{(u, \hat{\boldsymbol{\alpha}})\ s.t.\ \ u \in [0,1], \quad \|\hat{\boldsymbol{\alpha}}\| = 1\}$

- The value of $\hat{\boldsymbol{\alpha}}$ that **minimises the Hamiltonian at each instant corresponds to the Primer Vector [26]** → $\hat{\boldsymbol{\alpha}}^* = -\dfrac{\boldsymbol{\lambda}_v}{\|\boldsymbol{\lambda}_v\|}$

- Substituting the Primer Vector in the Hamiltonian yields [25]:

$$H(\boldsymbol{s}, \boldsymbol{\lambda}, u) = 1 + \boldsymbol{\lambda}_r \cdot \boldsymbol{v}_{s/c} - \frac{\mu_S}{r_{s/c}^3} \boldsymbol{r}_{s/c} \cdot \boldsymbol{\lambda}_v + \frac{T_{max}}{I_{sp} g_0} u \left(- \frac{\lambda_v}{m_{s/c}} I_{sp} g_0 - \lambda_m \right)$$

$$u^* = \begin{cases} 0 & \text{if } S_t > 0 \\ 1 & \text{if } S_t < 0 \end{cases}$$

Swtiching function for time-optimal problem → $S_t < 0$ → $u^* = 1$

[24] L. S. Pontryagin, The Mathematical Theory of Optimal Processes. London: Routledge, 1987. ISBN: 978-2881240775.
[25] C. Zhang, F. Topputo, F. Bernelli-Zazzera, Y.-S. Zhao, Journal of Guidance, Control, and Dynamics, vol. 38, no. 8, 2015. DOI: https://doi.org/10.2514/1.G001080.
[26] R. P. Russell, Journal of Guidance, Control, and Dynamics, vol. 30, no. 2, pp. 460–472, 2007. DOI: https://doi.org/10.2514/1.22984.

Appendix – Time-optimal low-thrust trajectory

- **Time-optimal solution for rendezvous transfer**
- **Lagrange multipliers in transversality condition:** $\boldsymbol{\lambda}^*(t_{arr}) = [\boldsymbol{\lambda}_r(t_{arr})\ \boldsymbol{\lambda}_v(t_{arr})]^T$.

→ $$R(\boldsymbol{\lambda}_0,\ t_{arr}) = \begin{cases} \boldsymbol{s}^*(t_{arr}) - \boldsymbol{\psi}(t_{arr}) = 0 \\ \lambda_m(t_{arr}) = 0 \\ H(t_{arr}) - \boldsymbol{\lambda}^*(t_{arr}) \cdot \dot{\boldsymbol{\psi}}(t_{arr}) = 0 \end{cases}$$

Transversality condition [27]

- **The problem is adimensionalised** → Reference units:

$\mathrm{MU} = m_{s/c_0}$

$\mathrm{LU} = 1\ \mathrm{AU}$

$$GM = \mu_S \frac{\mathrm{TU}^2}{\mathrm{LU}^3} = 1 \implies \mathrm{TU} = \sqrt{\frac{\mathrm{LU}^3}{\mu_S}}$$

- **Zeros of the function** $R(\boldsymbol{\lambda}_0,\ t_{arr})$ → **MATLAB's *fsolve*** inside a while loop with a maximum number of iterations.

Initial guess for the initial co-states value and the arrival time: $[\boldsymbol{\lambda}(t_0)\ \ t_{arr}]^T$ → **Initial guess refinement process**

- **Sensitivity analysis of co-states initial values** that grant convergence as a function of departure time over the launch window.
- **Shape-based low-thrust trajectory launch date,** t_0 → Extract from the sensitivity analysis the associated restricted range of Lagrange multipliers values from which find the converging initial guess on $\boldsymbol{\lambda}(t_0)$.
- **Shape-based low-thrust trajectory launch date,** t_0**, and Time of Flight,** $\mathrm{ToF}_{\mathrm{SB}}$ → Initial guess on t_{arr}.

[27] J. T. Betts, Journal of guidance, control, and dynamics, vol. 21, no. 2, pp. 193–207, 1998. DOI: https://doi.org/10.2514/2.4231.

Appendix – Time-optimal low-thrust trajectory

Selected mission

Pareto-optimal solution maximising the deflection.

Time-optimal low-thrust trajectory algorithm

Pontryagin Maximum Principle (PMP) [24].

Refined initial guess on arrival time and co-states → Shape-based low-thrust trajectory: t_0, m_{s/c_0}, $\Delta \boldsymbol{V}_{s/c}$, Time of Flight ($\mathrm{ToF}_{\mathrm{SB}}$).

Optimised mission feasibility

$$m_{str} \geq 0.13\, m_{s/c_0}$$

$$m_{f_{stored}} \leq 0.65\, m_{s/c_0}$$

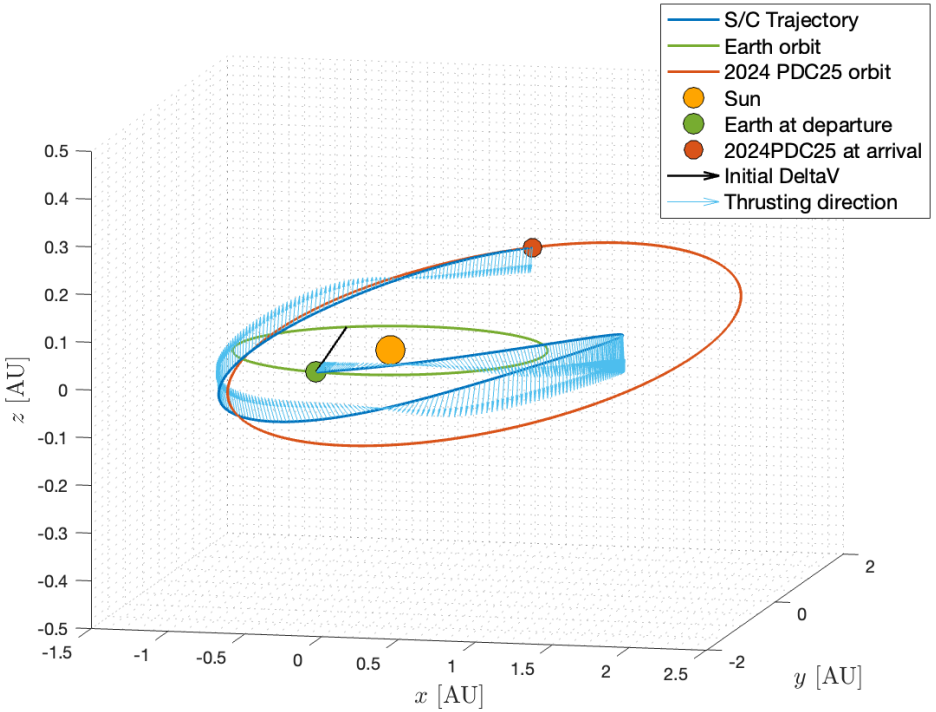

Checks to ensure time-optimality

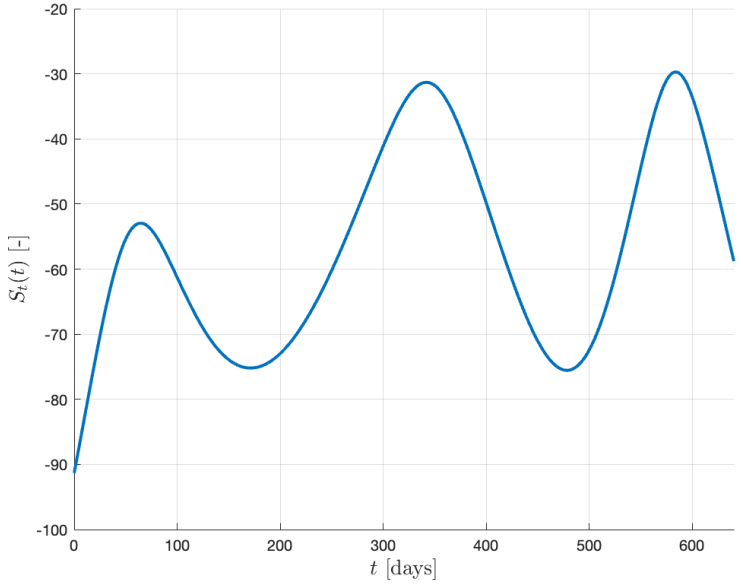

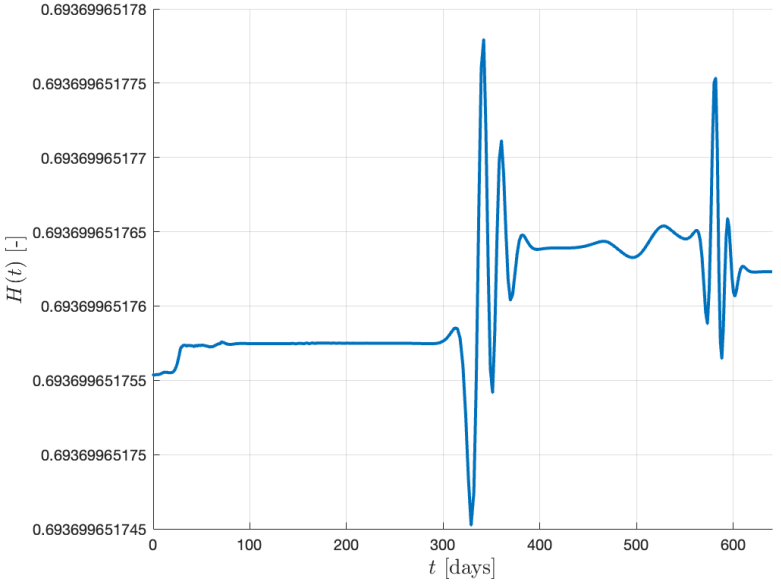

[24] L. S. Pontryagin, The Mathematical Theory of Optimal Processes. London: Routledge, 1987. ISBN: 978-2881240775.

Appendix – Formation orbits design

- **Spacecraft in close-proximity of the asteroid** → Linearised Proximal motion equations, with **condition for periodic motion [28]:** $\delta a_{FF} = 0$.

- **Optimisation variables** → $\delta\boldsymbol{\alpha}_{FF} = [\,\delta a_{FF}\ \delta e_{FF}\ \delta i_{FF}\ \delta\Omega_{FF}\ \delta\omega_{FF}\ \delta M_{FF}]^T$

- **Spacecraft relative position vector rotated in TNH frame** → $\delta\boldsymbol{r}_{s/c_{TNH}} = \left[\delta x_{s/c_{TNH}}\ \ \delta y_{s/c_{TNH}}\ \ \delta z_{s/c_{TNH}}\right]^T$

- **Multi-objective optimisation [28]** →

$$\min_{\delta\boldsymbol{\alpha}_{FF}\in D}\ \max_{\theta}\ J_1 = \delta r$$

$$\min_{\delta\boldsymbol{\alpha}_{FF}\in D}\ \max_{\theta}\ J_2 = -\tan^{-1}\left(\frac{\sqrt{x_{s/c_{TNH}}^2 + z_{s/c_{TNH}}^2}}{y_{s/c_{TNH}}}\right)$$

- **Control law [28]** → $\boldsymbol{u}(t) = -\left(-\frac{\mu_A}{\delta r_{s/c}^3}\delta\boldsymbol{r}_{s/c} + \frac{\boldsymbol{F}_s}{m_{s/c}(t)}\right) - C_d\delta\boldsymbol{v}_{s/c}$

MLA constraints

$$\begin{cases} C_{ineq_1,MLA} = y_{lim} - \min_{\theta}\ |y(\theta)| \le 0 \\ C_{ineq_2,MLA} = \max_{\theta}\ |y(\theta)| - 1.5\ y_{lim} \le 0 \end{cases}$$

MIBD constraints

$$\begin{cases} C_{ineq_1,MIBD} = 0.7\ r_{max} - \min_{\theta}\ \left|\delta r_{s/c}(\theta)\right| \le 0 \\ C_{ineq_2,MIBD} = \max_{\theta}\ \left|\delta r_{s/c}(\theta)\right| - r_{max} \le 0 \end{cases}$$

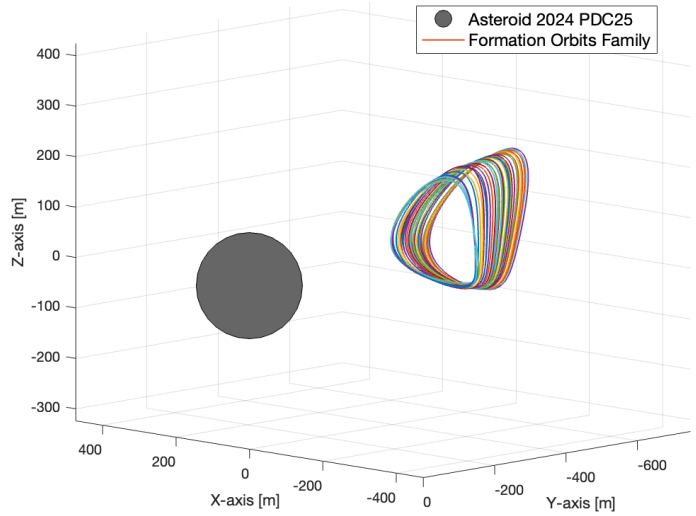

Example of formation orbits family for MLA.

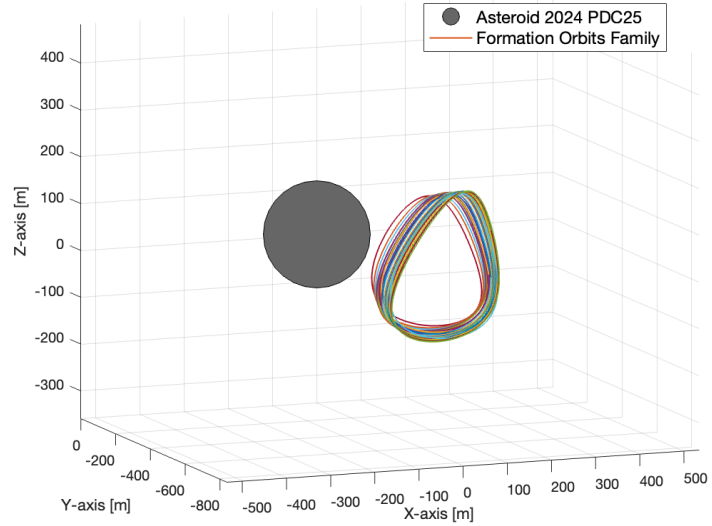

Example of formation orbits family for MIBD.

[28] M. Vasile and C. A. Maddock, Advances in space research, vol. 50, no. 7, pp. 891–905, 2012. DOI: https://doi.org/10.1016/j.asr.2012.06.001.

Appendix – Subsystems mass estimation

Propulsion subsystem

- **NEXT-C thrusters used on DART mission [7]**
  - **High TRL** → Selected for mission design.
  - **Multiple units** → Assumed identical.
- **Thruster efficiency** → $\eta_T = \frac{F_{\max_1} I_{sp}\, g_0}{2\, P_{in_1,max}}$

$P_{in_1,max}\ [kW]$	$F_{max_1}\ [N]$	$I_{sp}\ [s]$	$\eta_T\ [-]$	$m_{thr_{dry}}\ [kg]$
7.78	0.235	4190	0.6208	50.00

NEXT-C thrusters main properties used in this study [7].

- **One NEXT-C thruster:** Mass of $14\ kg$ and Power Processing Unit mass of $36\ kg$ [7] → $m_{thr_{dry}} = 50\ kg$.
- **Total thrusters dry mass on board the spacecraft** → $m_{thr_{dry,tot}} = 2\, N_{pairs}\, m_{thr_{dry}}$
- **Deflection strategies require different amount of fuel for the close-proximity phase:**

	Nuc	SLA	MLA	GT	EGT	SIBD	MIBD
$m_{f_{prox}}\ [kg]$	$m_{f_{control}}$	$m_{f_{hover}}$	$m_{f_{control}}$	$m_{f_{hover}}$	$m_{f_{hover}} + m_{f_{gain}}$	$m_{f_{dev,SIBD}}$	$m_{f_{dev,MIBD}}$

- **Total fuel mass stored with a safety margin of 5% [29]** → $m_{f_{stored}} = 1.05\left(m_{f_{LT}} + m_{f_{prox}}\right) = 1.05\, m_{f_{tot}}$
- **Tanks mass [28]** → $m_{tanks} = 0.10\, m_{f_{stored}}$

[7] NASA, 2021. NASA's Evolutionary Xenon Thruster-Commercial (NEXT-C). NASA Technical Reports Server. URL: https://ntrs.nasa.gov/citations/20210024276.
[29] J. R. Wertz and W. J. Larson, Space Mission Analysis and Design. Springer, 1999. ISBN: 978-0792359012.

Appendix – Subsystems mass estimation

Solar Panels Design [29] – Part 1

1. **Power requirement at 1 AU that must be produced by the solar arrays, P_{sa}:**
   - **For all models except SLA and MLA:** Thrusters maximum input power → $P\_sa = 2\, N_{pairs}\, P_{in_{\max_1}}$
   - **For SLA and MLA models:** Sum of laser input power requirement at 1 AU, and power needed by the thrusters for hovering or maintaining formation flight, at 1 AU → $P_{sa} = P_{L,1AU} + P_{req,control}$
2. **Beginning of Life (BOL) Power capability specific per unit area:**

Specific power output at 1 AU [29]:
$P_0 = \varepsilon_{BOL}\, I_0$

Inherent Degradation factor [29]:
$I_d = 0.88$

$P_{BOL_{spec}} = P_0\, I_d\, cos(\theta)$

Solar cells efficiency at BOL [29] → $\varepsilon_{BOL} = 0.3$
Solar Irradiance at 1 AU → $I_0 = 1361\ W/m^2$

Average inclination angle between solar array surface normal and Sun direction:
Unknown a priori → Angle between equatorial and ecliptic plane used as critical case [29]: $\theta = 23.44°$

[29] J. R. Wertz and W. J. Larson, Space Mission Analysis and Design. Springer, 1999. ISBN: 978-0792359012.

Appendix – Subsystems mass estimation

Solar Panels Design [29] – Part 2

3. From $P_{BOL_{spec}}$, the solar cells degradation per year (dpy) and mission duration → **Solar cells lifetime degradation [29].**

- **For all models except SIBD and MIBD →** Nominal solar cells degradation per year [29]: $dpy_{nom} = 0.01$.

Lifetime degradation during transfer

$$L_{life_{transfer}} = (1 - dpy_{nom})^{TOF_{yrs}}$$

Lifetime degradation during deflection

$$L_{life_{dev}} = (1 - dpy_{nom})^{t_{def_{yrs}}}$$

- **For SIBD and MIBD models →** To consider contamination of solar panels due to back-sputtering, the solar cells dpy during the deflection action is doubled: $dpy_{def} = 2\, dpy_{nom} = 0.02$.

Lifetime degradation during transfer

$$L_{life_{transfer}} = (1 - dpy_{nom})^{TOF_{yrs}}$$

Lifetime degradation during deflection

$$L_{life_{dev}} = (1 - dpy_{def})^{t_{def_{yrs}}}$$

4. The solar array specific power, per unit area, produced at Beginning of Deflection (BOD) and at End of Life (EOL) [29]:

- **Solar array specific power at BOD →** $P_{BOD_{spec}} = L_{life_{transfer}}\, P_{BOL_{spec}}$
- **Solar array specific power at EOL →** $P_{EOL_{spec}} = L_{life_{dev}}\, P_{BOD_{spec}}$

5. The solar array surface area to respect the power requirement until EOL [29] →

$$A_{sa_{tot}} = P_{sa}/P_{EOL_{spec}}$$

$$A_{sa_{wing}} = A_{sa_{tot}}/2$$

[29] J. R. Wertz and W. J. Larson, Space Mission Analysis and Design. Springer, 1999. ISBN: 978-0792359012.

Appendix – Subsystems mass estimation

Solar Panels Design [29] – Part 3 & Radiators design

6. **The actual generated power at 1 AU $[W]$:**
   - **At BOL →** $P_{1AU_{BOL}} = P_{BOL_{spec}} A_{sa_{tot}}$
   - **At BOD →** $P_{1AU_{BOD}} = P_{BOD_{spec}} A_{sa_{tot}}$
   - **At EOL →** $P_{1AU_{EOL}} = P_{EOL_{spec}} A_{sa_{tot}}$

$P_{sa}[kW]$	$M_{sa}\,[kg]$	$A_{sa_{tot}}[m^2]$	$A_{sa_{wing}}[m^2]$
46.68	485.04	176.56	88.28
83.41	783.06	285.05	142.53
93.36	967.07	352.03	176.02

Examples of solar array sizing for some power levels used.

7. **Roll-Out Solar Array (ROSA) used on DART mission [30]:**
   - **High TRL →** Selected for mission design.
   - **Power-to-mass ratio of** $P_{to_{Mass}} = 120\ W/kg$ **→ Solar array mass →** $M_{sa} = P_{1AU_{BOL}} / P_{to_{Mass}}$

Radiators designed to dissipate the excess power generated throughout the mission **→ Radiators properties [10]**

- **Sized to dissipate maximum excess power → Occurs at BOL** , when solar panels produce the peak power output.

Stefan-Boltzmann constant: $\sigma_{SB} = 5.6704 \times 10^{-8}\ W/m^2K^4$

$$m_{rad} = \frac{\rho_R\,(P_{1AU_{BOL}} - P_{sa})}{\sigma_{SB}\,\varepsilon_R\,T_R^4}$$

Radiators density: $\rho_R = 5.0\ kg/m^2$

Radiators operating temperature: $T_R = 283\ K$

Radiators emissivity: $\varepsilon_R = 0.8$

[29] J. R. Wertz and W. J. Larson, Space Mission Analysis and Design. Springer, 1999. ISBN: 978-0792359012.

[30] Redwire Space, 2023. URL: https://redwirespace.com/wp-content/uploads/2023/06/ redwire-roll-out-solar-array-flysheet.pdf.

[10] M. Vasile, A. Gibbings, I. Watson, and J.-M. Hopkins, Acta Astronautica, vol. 103, pp. 382–394, 2014. DOI: https://doi.org/10.1016/j.actaastro.2014.01.033.

Appendix – Subsystems mass estimation

Specific design for Laser Ablation models [10]

- **Specific power requirement at 1 AU for LA strategies →** $P_{sa} = P_{L,1AU} + P_{req,control}$
- **During the low-thrust trajectory to reach the asteroid, the laser system is not operating:**
  - Solar array produced power fully allocated to the six thrusters used during the transfer trajectory.
  - Feasible approach because of sufficiently high laser power requirement.
- **Once the laser system is operational,** thrusters used to keep the proximity configuration → $P_{req,control} = \frac{F_{req}\, I_{sp}\, g_0}{2\, \eta_T}$
  - **For SLA model →** $F_{req} = T_{hover}$
  - **For MLA model →** $F_{req} = T_{control}$
- **For the LA strategies, mass of laser plus the optics subsystem [10] →** $m_L = \alpha_L\, P_{L,1AU}$
  - Specific mass of the laser plus optics [10]: $\alpha_L = 0.01\ kg/W$
- **Radiators mass estimation specific for LA strategies [10] →** $m_{rad_{LA}} = \frac{\rho_R\,(1-\eta_L)\,P_{L,1AU}}{\sigma_{SB}\varepsilon_R T_R^4}$
  - Laser system efficiency [10]: $\eta_L = 0.55$.

[10] M. Vasile, A. Gibbings, I. Watson, and J.-M. Hopkins, Acta Astronautica, vol. 103, pp. 382–394, 2014. DOI: https://doi.org/10.1016/j.actaastro.2014.01.033.

Appendix – Subsystems mass estimation

Specific design for Nuclear deflection model

1. The warhead mass of each NED, $m_{wh_{NED}}$, with an additional a 10% margin [4] → $$m_{wh_{NED}} = 1.10 \frac{E_t}{YTW}$$
   - **Total energy carried by each NED** → $E_t = 0.2 - 0.4\ Mt$ in this thesis.
   - **Yield-To-Weight ratio** → $YTW = 1.8\ kton/kg$, selected in accordance with NASA team at SMPAG.
2. Given the number of NEDs, N_{NEDs}, **the total warhead mass** on board the "Carrier" spacecraft → $m_{wh_{tot}} = N_{NEDs}\, m_{wh_{NED}}$
3. Warhead mass is 30% of m_{NED} [4]: $m_{NED} = \frac{m_{wh_{NED}}}{0.30}$ → 70% for structure and payloads → $m_{str_{NED}} = 0.70\, m_{NED}$
4. To ease the design of multiple NEDs, **all devices are assumed identical** → **Total NEDs mass** → $m_{NEDs_{tot}} = N_{NEDs}\, m_{NED}$
5. The total mass of structure & payloads subsystem for all NEDs → $m_{str_{NEDs}} = 0.70\, m_{NEDs_{tot}}$
6. Once all subsystems masses are computed, they are expressed in percentage of m_{sc0} and subtracted from unity to obtain the remaining percentage of m_{s/c_0} allocated to the "Carrier" spacecraft structure and payloads subsystem → $m_{str_{Carrier}}$.
7. **To ensure feasibility of missions design** → Optimisation constraint imposed on $m_{str_{Carrier}}$ → $m_{str_{Carrier}} \geq 0.13\, m_{s/c_0}$

[4] J. P. Sanchez, C. Colombo, M. Vasile, G. Radice, Journal of Guidance, Control, and Dynamics, vol. 32, no. 1, pp. 121–142, 2009. DOI: https://doi.org/10.2514/1.36774.

Appendix – Launcher selection

- Falcon Heavy in Expendable configuration enables to launch a larger maximum m_{s/c_0} for the same C_3 value compared to the Recoverable one, but it has a higher cost per launch.

Asteroid impact threat scenario:

- Cost is not the main driver
- Currently best performing launcher can be selected.

Falcon Heavy in Expendable configuration

$C_3 \leq 25\ km^2/s^2$ → Ensure sufficient m_{s/c_0}

- Accommodate up to 13 NEDs;
- High-power laser system;
- Large amount of fuel for IBD;
- Deliver large mass for GT and EGT.

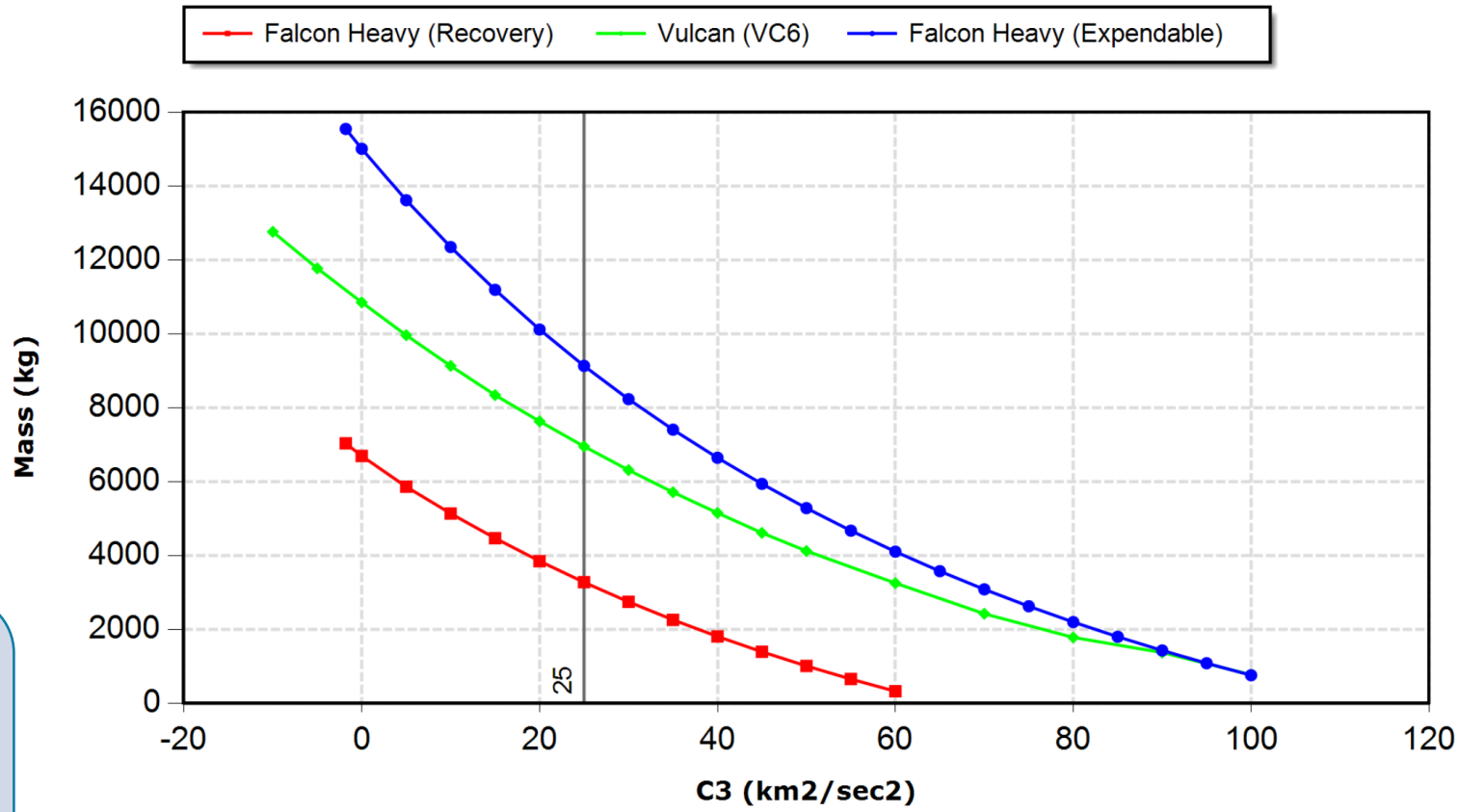

Performance comparison among several launchers [3].

[3] NASA Launch Services Program, 2025. URL: https://elvperf.ksc.nasa.gov/Pages/Default.aspx.

APPENDIX – DEFLECTION MISSIONS

Stand-off NEDs in "Carrier" configuration

- **One or more NEDs on board a "Carrier" spacecraft.**
- **Arrival constraint** → $4 - 23$ months before perihelion.
- **NEDs individually deployed from the "Carrier".**
- **NEDs detonations:**
  - Far side of the asteroid [8] → Spacecraft shielded.
  - Symmetrically around perihelion.
  - Time separation of 14 days [6].

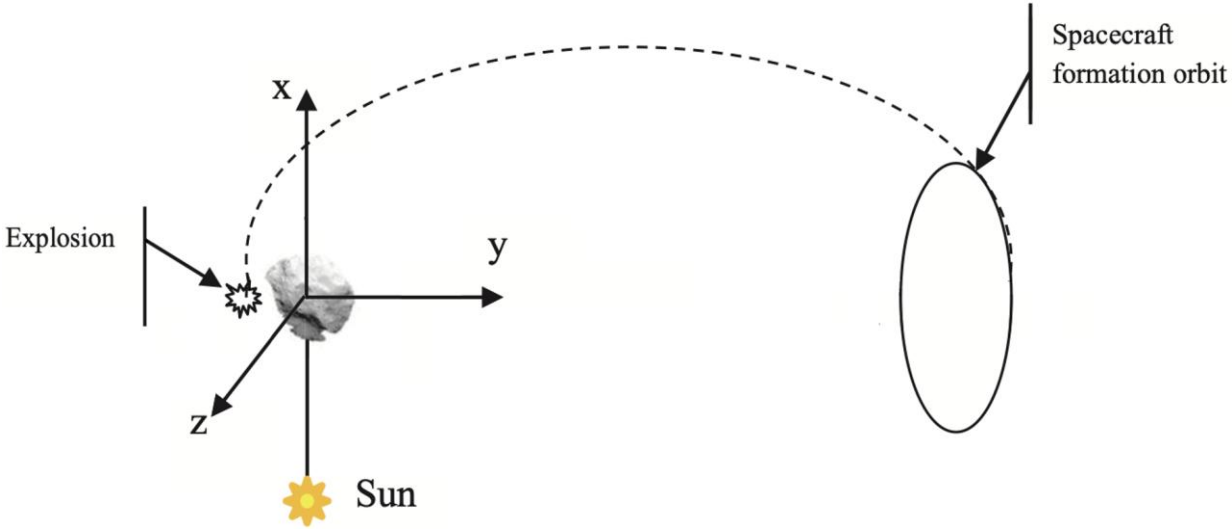

Stand-off detonations in "Carrier" configuration scheme [8].

- The δv_{Nuc} from a nuclear stand-off explosion [4][8]:

$$\delta v_{Nuc} = \delta v_{gamma} + \delta v_{X-rays} + \delta v_{neutrons} + \delta v_{debris}$$

- **To avoid undesired fragmentation of the asteroid:**

$$\beta = 2 \implies \delta v_{Nuc} \leq 4\%\, v_{esc}$$

Stand-off detonation distance, H, influences δv_{Nuc} → **Optimisation variable**

[6] N. Chabot, E. Adams, A. Rivkin, and J. Kalirai, Acta Astronautica, vol. 220, pp. 118– 125, 2024. DOI: https://doi.org/10.1016/j.actaastro.2024.04.001.
[8] M. Vasile and N. Thiry, Advances in Space Research, vol. 57, no. 8, pp. 1805–1819, 2016. DOI: https://doi.org/10.1016/j.asr.2015.11.036.

5 x 0.4 Mt NEDs – Early & Primary missions

	Launch	Arrival	ToF $[days]$	C_3 $[km^2/s^2]$	m_{s/c_0} $[kg]$	$m_{f_{LT}}$ $[kg]$	H $[m]$	δv $[\% \, v_{esc}]$	δb $[\% \, C]$
Lowest Mass	2029-06-16	2031-04-13	665.11	15.03	10950.27	1971.26	426.92	3.943	**73.03**
	2031-05-08	2032-11-25	567.24	14.36	10655.27	1681.18	426.96	3.807	**52.94**
50th percentile	2029-06-16	2031-04-12	664.50	13.96	10754.72	1969.46	423.86	3.997	**101.91**
	2031-05-08	2032-11-23	565.61	15.22	10775.73	1676.36	423.86	4.000	**76.59**
Highest Mass	2029-06-16	2031-04-23	675.20	14.42	11123.02	2001.15	418.15	3.999	**134.56**
	2031-05-08	2033-11-20	561.93	13.87	10779.79	1665.44	418.14	4.000	**101.05**

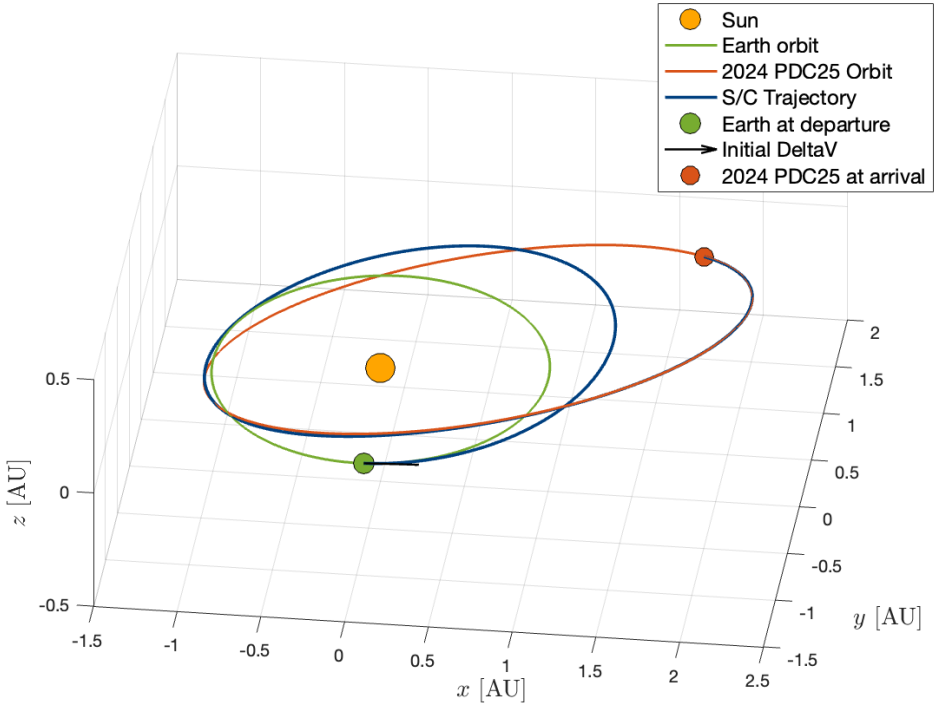

50th percentile
Early mission

Perihelion of
1st November 2032

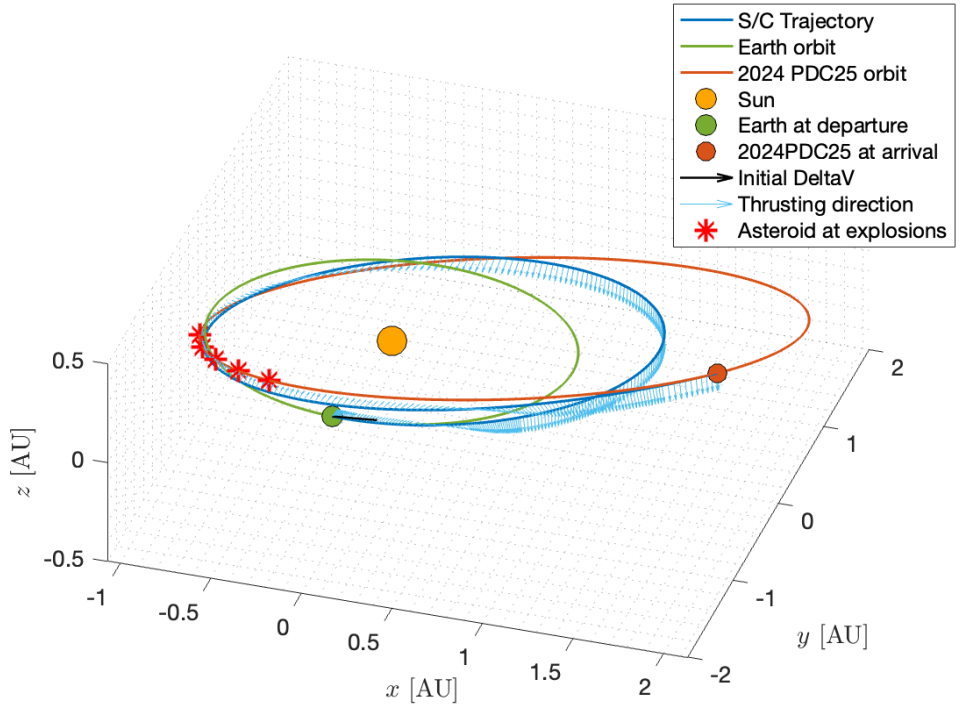

7 x 0.3 Mt NEDs – Early, Primary, Secondary missions

	Launch	Arrival	ToF $[days]$	C_3 $[km^2/s^2]$	m_{s/c_0} $[kg]$	$m_{f_{LT}}$ $[kg]$	H $[m]$	δv $[\% v_{esc}]$	δb $[\% C]$
Lowest Mass	2029-06-16	2031-04-06	658.79	15.46	10971.90	1952.51	364.81	3.987	**101.95**
	2031-05-08	2032-12-06	578.48	13.61	10972.04	1714.49	364.80	3.998	**76.76**
	2033-06-19	2035-03-14	632.39	17.67	10498.68	1874.29	364.80	4.000	**51.14**
50th percentile	2029-06-16	2031-04-12	664.63	15.94	10813.41	1969.84	362.11	3.999	**140.81**
	2031-05-08	2032-11-21	563.45	15.22	10819.65	1669.94	362.12	3.985	**105.34**
	2033-06-19	2035-03-03	622.06	18.60	10377.72	1843.66	362.11	3.993	**70.29**
Highest Mass	2029-06-16	2031-05-13	695.74	12.95	11212.94	2062.04	357.01	4.000	**185.82**
	2031-05-08	2032-11-20	562.28	15.51	10715.74	1666.50	357.01	4.000	**139.52**
	2033-06-19	2035-03-12	630.32	17.27	10406.01	1868.15	357.03	3.991	**92.70**

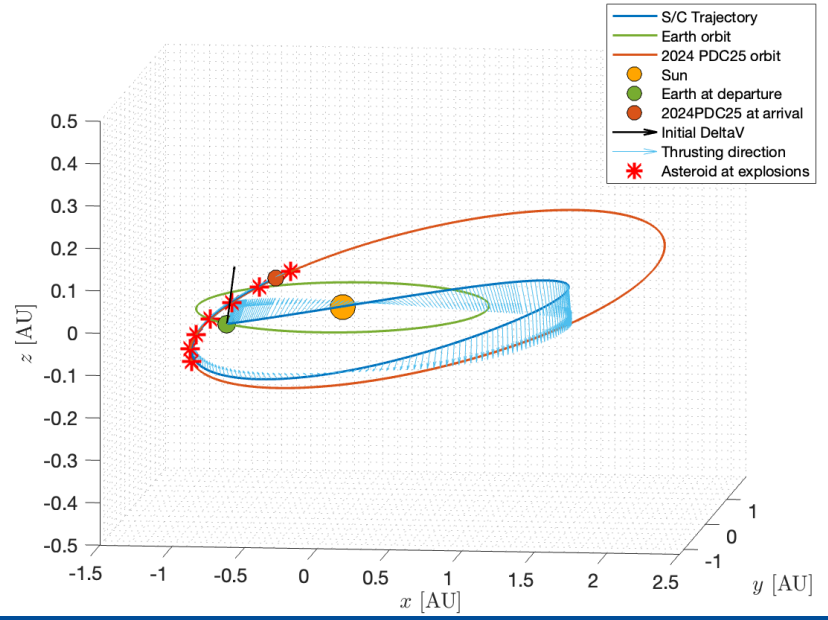

Lowest Mass case
Primary mission

Perihelion of
15th December 2034

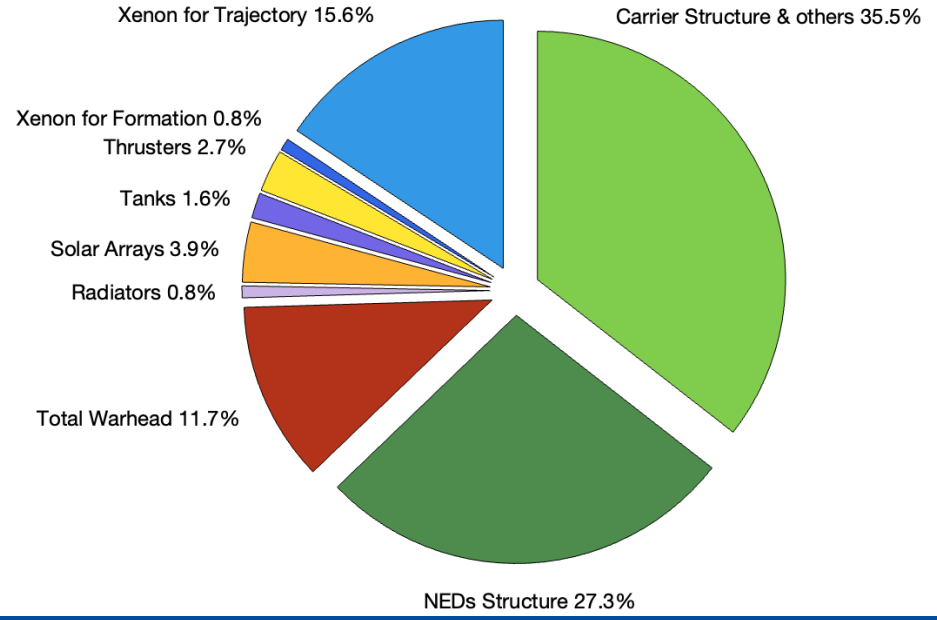

9 x 0.3 Mt Secondary & 13 x 0.2 Mt Late campaigns

	Launch	Arrival	ToF $[days]$	C_3 $[km^2/s^2]$	m_{s/c_0} $[kg]$	$m_{f_{LT}}$ $[kg]$	N_{NEDs} $[-]$	H $[m]$	δv $[\% v_{esc}]$	δb $[\% C]$
Lowest Mass	2033-06-19	2035-03-09	627.45	18.11	10326.17	1859.65	9	364.80	3.999	64.65
	2035-06-08	2037-06-24	747.02	15.03	11170.07	2214.01	13	292.10	3.995	41.25
50th percentile	2033-06-19	2035-02-20	610.57	18.80	10254.95	1809.61	9	362.11	3.994	88.89
	2035-06-16	2037-08-18	794.55	14.09	11369.66	2354.89	13	289.79	3.994	56.77
Highest Mass	2033-06-19	2035-02-20	611.11	18.90	10246.73	1811.21	9	357.02	3.993	115.24
	2035-06-16	2037-08-11	787.49	14.38	11316.66	2333.96	13	285.42	3.990	74.83

Highest Mass case Secondary → Perihelion of 27th January 2037

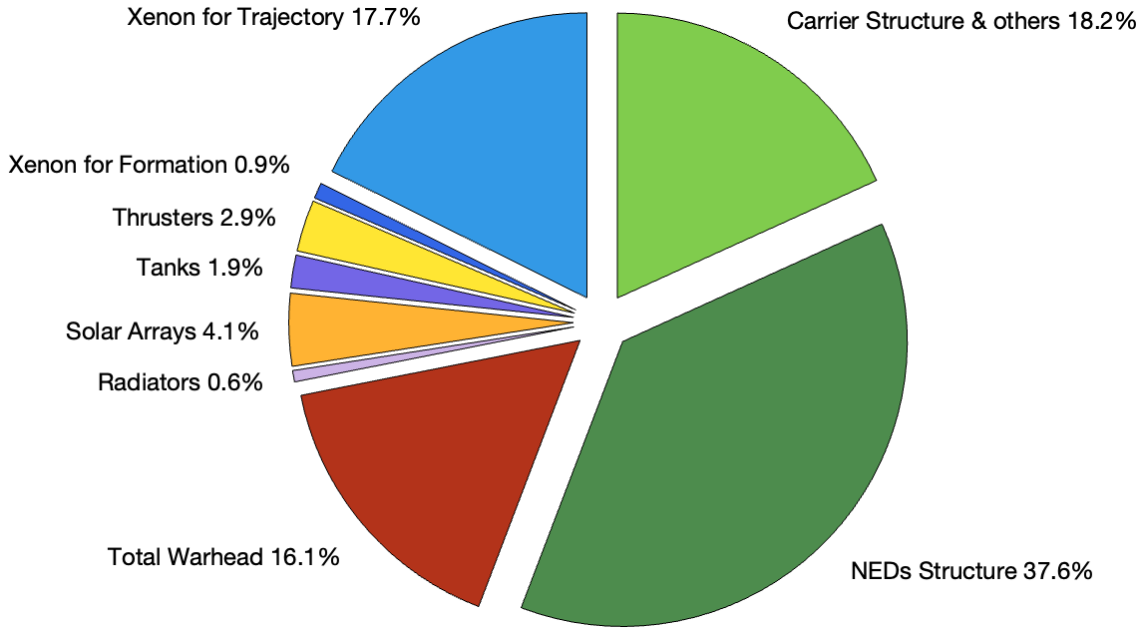

Highest Mass case Late → Perihelion of 12th March 2039

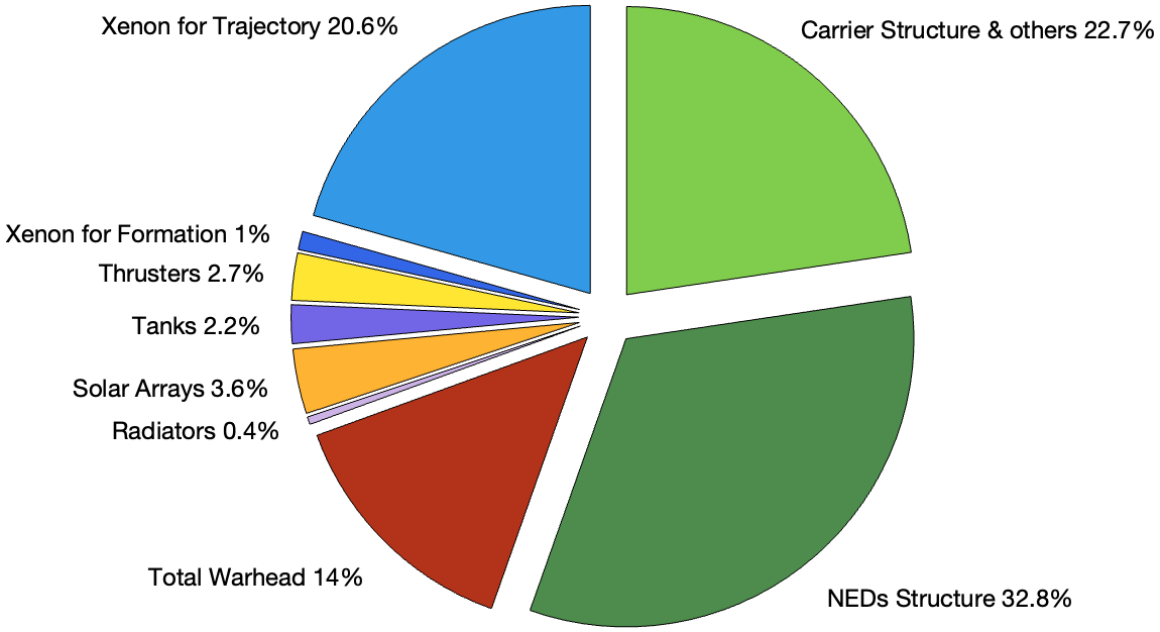

Single and Multiple Ion Beam Deflection

To avoid inefficient fuel expenditure

- Thrusters throttle down to half power.
- Deflection in arcs around each perihelion.

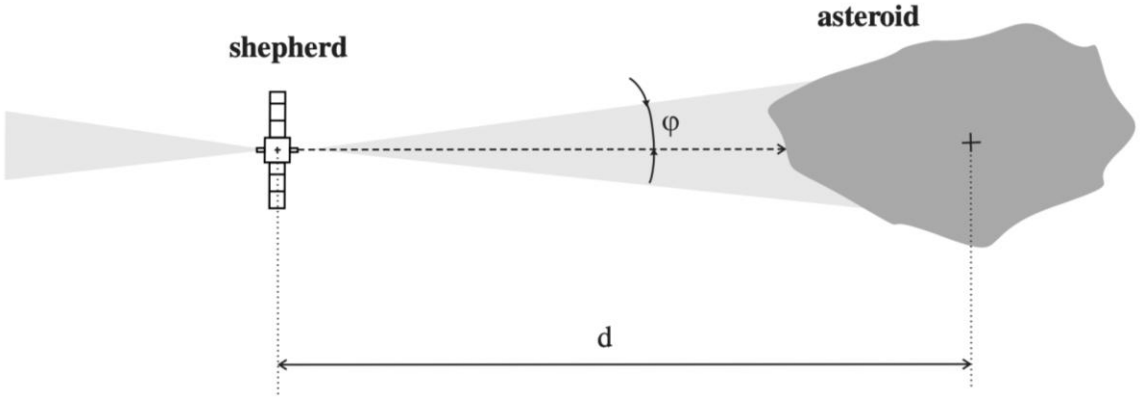

Scheme of IBD spacecraft hovering [9].

Multiple pairs of ion thrusters → Number of thruster pairs, N_{pairs}

Multiple IBD spacecraft → Number of spacecraft, $N_{s/c}$

→ **Optimisation variables**

Perturbing force in TNH frame:

$$\boldsymbol{F}_{IBD}(t) = -N_{pairs} \sum_{i=1}^{N_{s/c}} \boldsymbol{F}_{p1,\,i}(t)$$

→ **Spacecraft gravitational pull on the asteroid**

$$\boldsymbol{a}(t) = \boldsymbol{F}_{IBD}(t)/M_a - \boldsymbol{a}_{tug}(t)$$

[9] C. Bombardelli and J. Peláez, Journal of Guidance, Control, and Dynamics, vol. 34, no. 4, pp. 1270–1272, 2011. DOI: https://doi.org/10.2514/1.51640.

Single IBD – Early & Primary campaigns

	Launch	Arrival	ToF $[days]$	C_3 $[km^2/s^2]$	m_{s/c_0} $[kg]$	N_{pairs} $[-]$	$m_{f_{LT}}$ $[kg]$	$m_{f_{dev}}$ $[kg]$	δb [% C]
Lowest Mass	2029-06-16	2031-10-14	849.22	6.45	12171.07	6	2516.93	4943.09	**153.75**
	2031-05-08	2032-11-19	560.82	13.25	10651.21	6	1662.17	4232.62	**114.00**
50th percentile	2029-06-16	2031-11-01	867.44	6.32	12416.02	6	2570.92	5003.13	**74.26**
	2031-05-08	2032-11-23	565.68	12.44	10363.90	6	1676.56	4254.51	**54.38**
Highest Mass	2029-06-16	2031-07-31	774.70	11.07	12176.69	6	2296.05	5160.34	**36.26**
	2031-05-08	2033-03-21	682.99	14.31	10484.13	6	2024.26	3908.76	**20.98**

Lowest Mass case Early mission

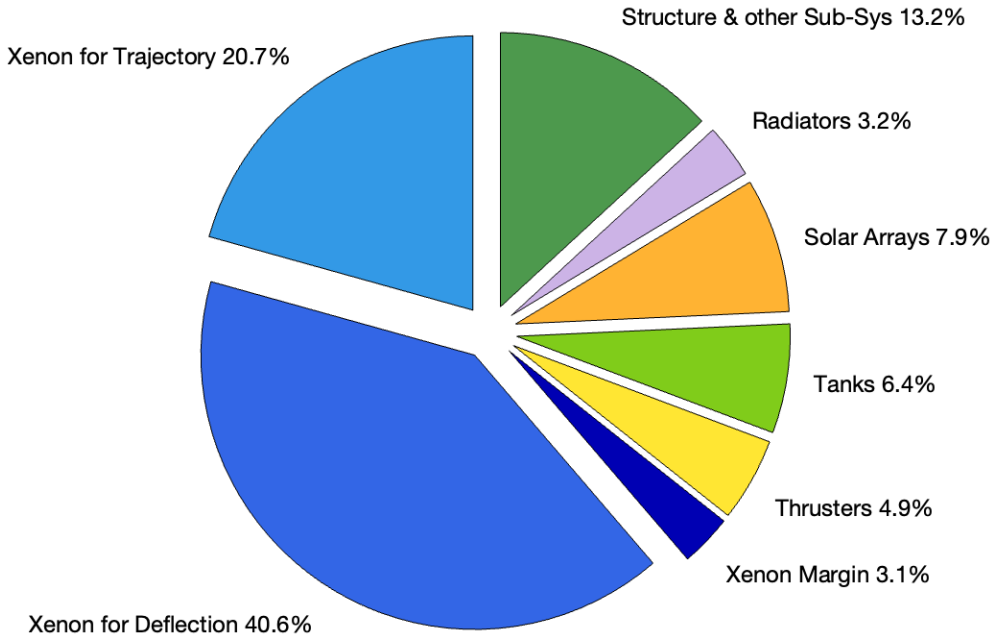

Highest Mass case Primary mission

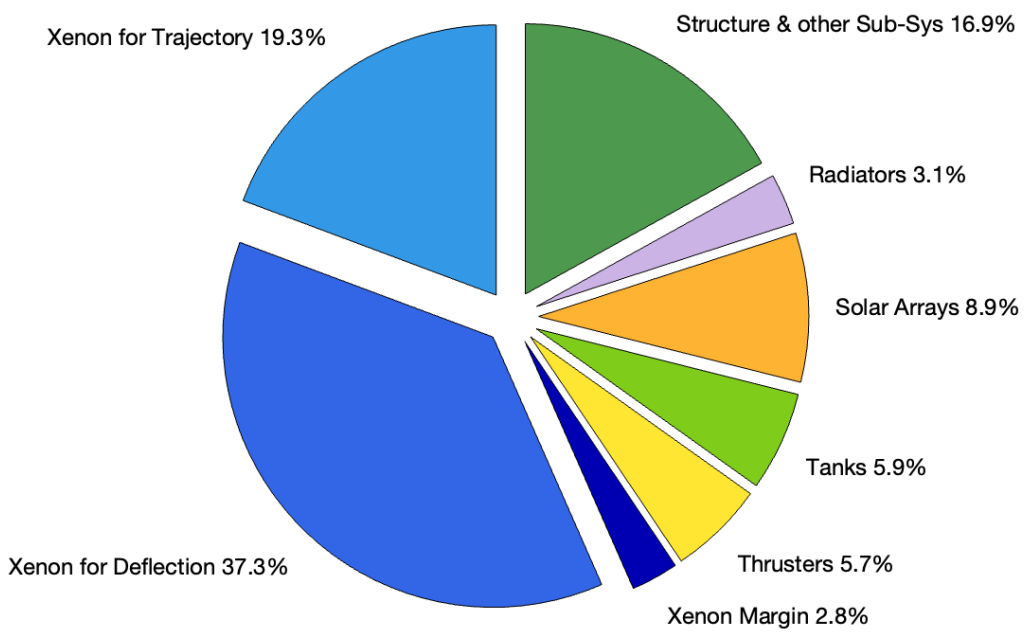

Multiple IBD – Early, Primary & Secondary missions

	Launch	Arrival	ToF $[days]$	C_3 $[km^2/s^2]$	m_{s/c_0} $[kg]$	N_{pairs} $[-]$	$N_{s/c}$ $[-]$	$m_{f_{LT}}$ $[kg]$	$m_{f_{dev}}$ $[kg]$	δb [% C]
Lowest Mass	2029-06-16	2031-04-25	677.85	15.48	10765.09	**3**	**2**	2009.02	2512.63	**145.93**
	2031-05-08	2033-05-25	748.01	6.09	11820.79	6	**2**	2216.96	3752.89	**174.46**
	2033-06-01	2035-09-27	847.84	5.87	11920.59	6	**3**	2512.82	2589.33	**127.82**
50th percentile	2029-06-16	2031-12-19	915.25	5.31	12483.36	6	**2**	2712.63	5001.03	**148.23**
	2031-05-08	2032-12-10	582.07	19.04	10304.53	6	**2**	1725.14	4161.43	**102.69**
	2033-06-01	2035-04-22	689.95	17.93	10475.57	6	**4**	2044.88	2658.40	**79.32**
Highest Mass	2029-06-06	2031-09-21	837.06	6.06	12413.23	6	**2**	2480.87	5103.30	**76.11**
	2031-05-08	2032-11-25	567.72	13.81	10680.19	6	**3**	1682.60	4339.17	**80.53**
	2033-06-01	2034-12-06	552.65	17.96	10427.69	6	**6**	1637.94	3327.22	**98.68**

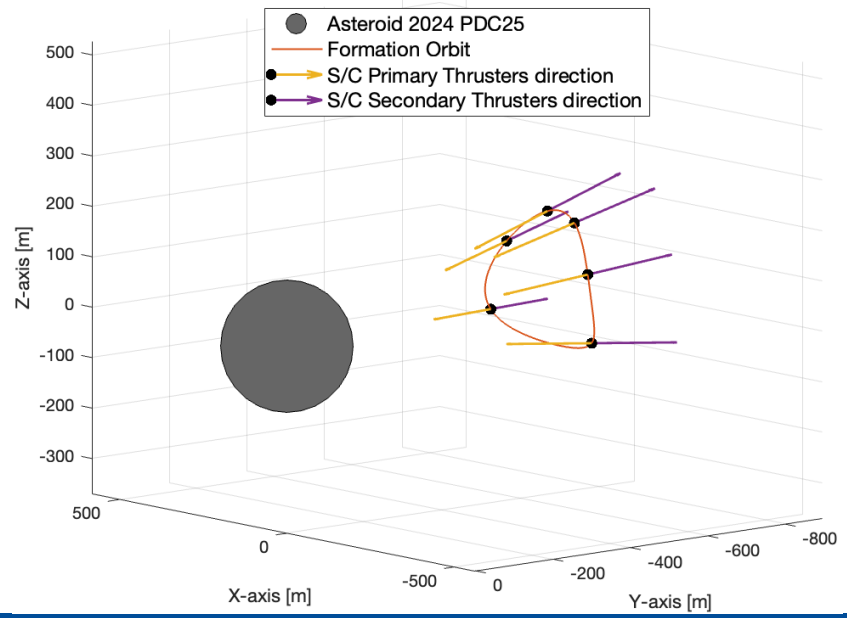

Highest Mass case
Secondary mission

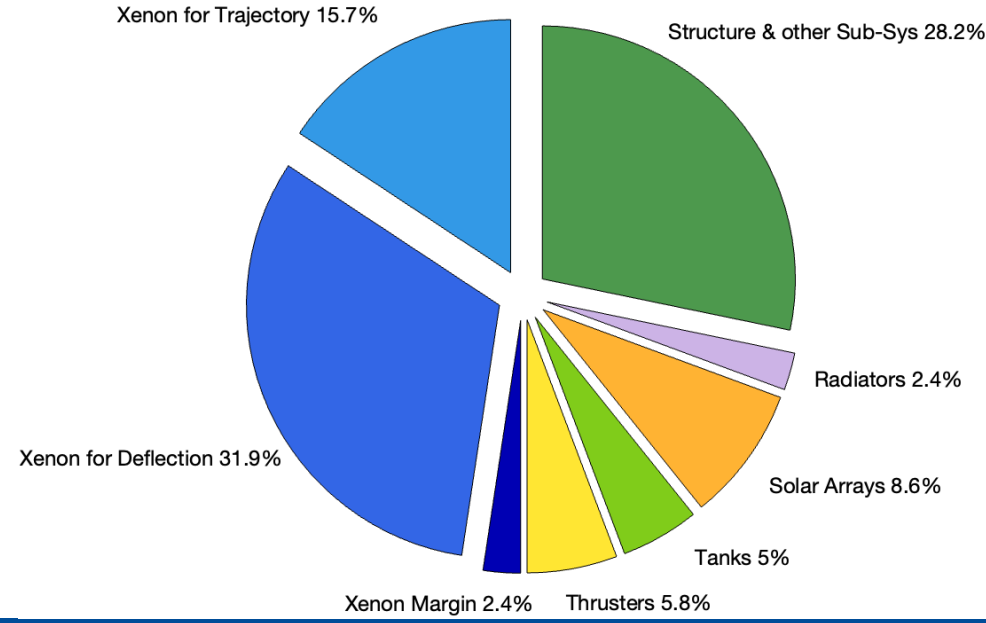

Single and Multiple Laser Ablation

- Continuous irradiation of a small portion of the asteroid surface [10].
- Ablated material forms a **plume of gas and ejecta:**

$$a_{sub}(t) = \frac{S_{sc}\ \bar{v}\ \dot{m}_{sub}(t)}{M_a(t)}$$

- Ablated material **re-condenses on exposed sensitive surfaces [10].**

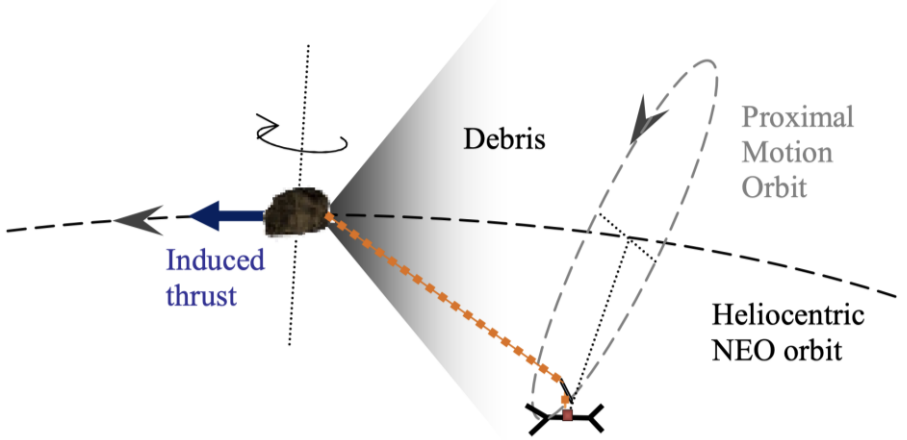

Laser Ablation in formation flight scheme [11].

Optimisation variables

- **SLA** → Hovering distance, d_{hover}
- **Laser input power at 1 AU,** $P_{L,1AU}$
- **MLA** → Spacecraft number, $N_{s/c}$

Sublimation acceleration in TNH frame:

$$\boldsymbol{a}_{sub}(t) = [\pm a_{sub}(t)\ \ 0\ \ 0]^T$$

Spacecraft gravitational pull on the asteroid

$$\boldsymbol{a}(t) = \boldsymbol{a}_{sub}(t) - \boldsymbol{a}_{tug}(t)$$

[10] M. Vasile, A. Gibbings, I. Watson, and J.-M. Hopkins, Acta Astronautica, vol. 103, pp. 382–394, 2014. DOI: https://doi.org/10.1016/j.actaastro.2014.01.033.
[11] A. Gibbings, J.-M. Hopkins, D. Burns, and M. Vasile, in IAA planetary defense conference, protecting Earth from asteroids: From threat to action, 2011.

Single LA – Two options of Early campaign

	Early campaign – Launch June 2029					
	Low hovering distance			High hovering distance		
	d_{hover} $[m]$	$P_{L,1AU}$ $[kW]$	δb $[\%\ C]$	d_{hover} $[m]$	$P_{L,1AU}$ $[kW]$	δb $[\%\ C]$
Lowest Mass	526.47	90.00	**29.91**	1127.68	90.29	**74.01**
50th percentile	443.92	90.51	**10.93**	1154.30	90.26	**35.65**
Highest Mass	535.83	90.67	**8.14**	1178.60	90.43	**19.35**

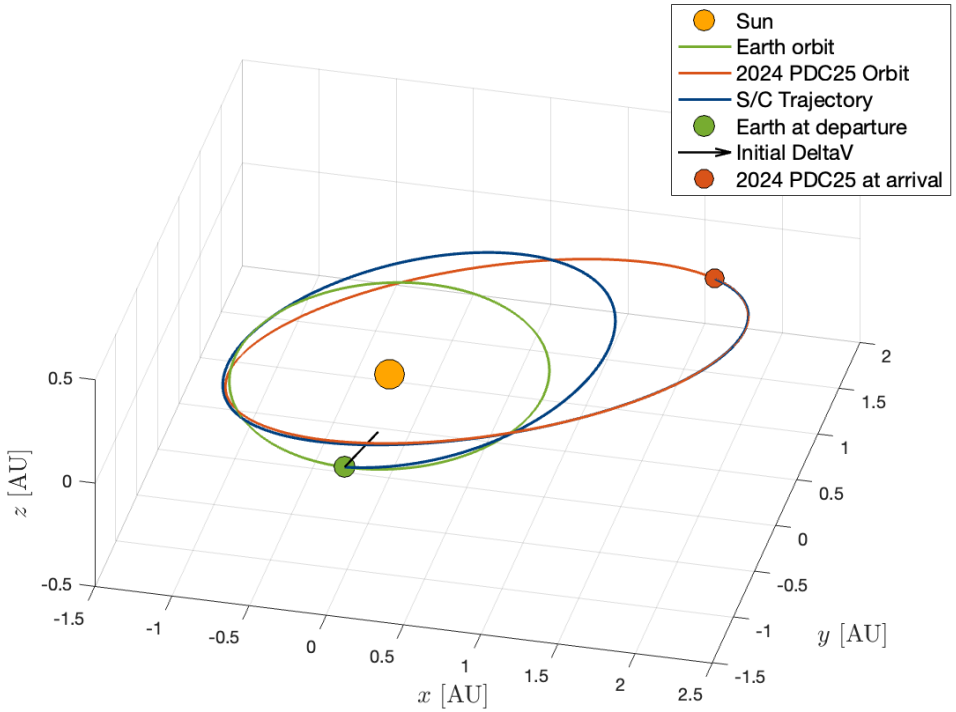

Lowest Mass High hovering distance case

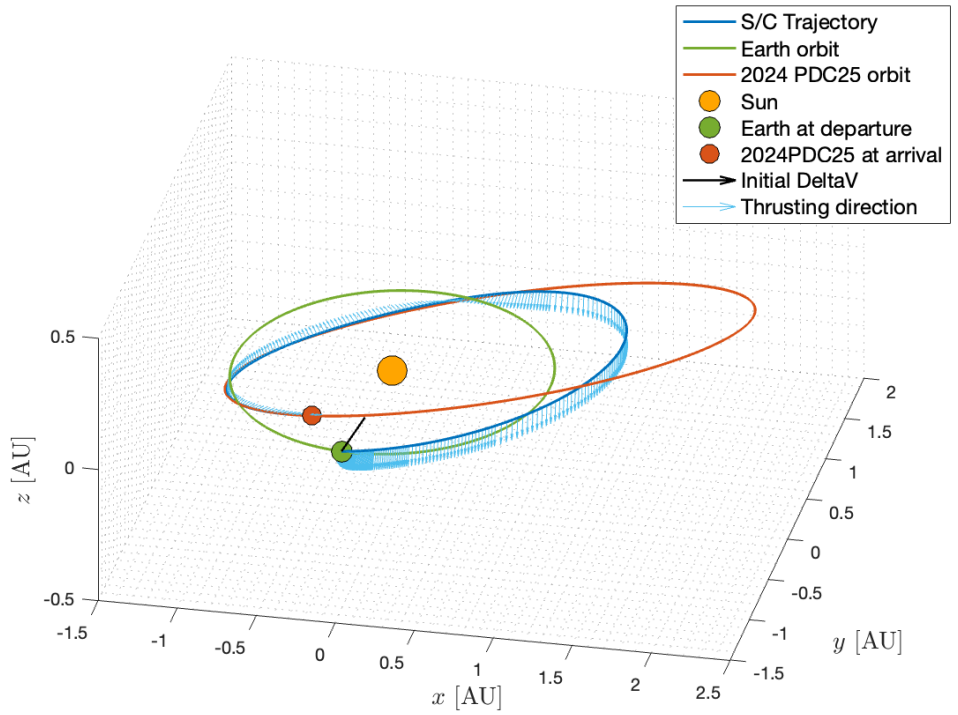

Single LA – Two options of Early campaign

	Launch	Arrival	ToF $[days]$	C_3 $[km^2/s^2]$	m_{s/c_0} $[kg]$	$m_{f_{LT}}$ $[kg]$	$P_{L,1AU}$ $[kW]$	d_{hover} $[m]$	δb [% C]
Lowest Mass	2029-06-16	2030-10-29	499.74	20.96	8321.96	1481.13	90.00	**526.47**	**29.91**
		2030-10-27	497.78	22.58	8401.83	1849.69	90.29	**1127.68**	**74.01**
50th percentile	2029-06-16	2030-11-21	523.00	24.20	8771.85	1550.08	90.51	**443.92**	**10.93**
		2030-12-11	542.19	21.56	9269.89	1606.94	90.26	**1154.30**	**35.65**
Highest Mass	2029-06-06	2030-11-09	511.01	22.56	8608.10	1514.52	90.67	**535.83**	**8.14**
		2031-02-07	601.04	22.77	9244.37	1781.35	90.43	**1178.60**	**19.35**

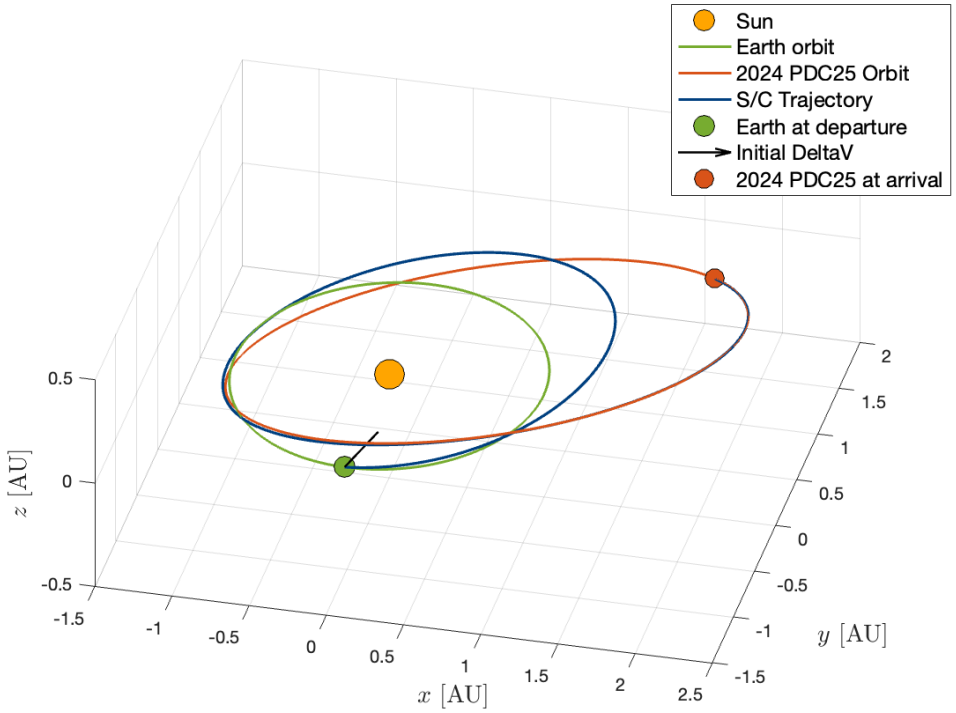

Lowest Mass
High hovering distance case

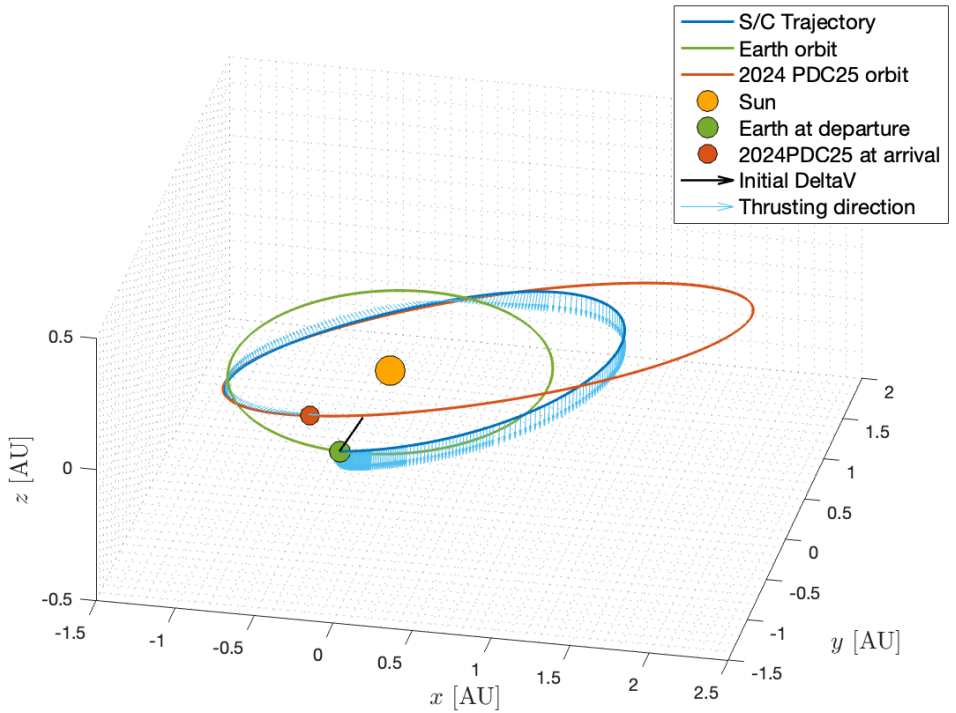

Multiple LA – Early, Primary & Secondary missions

	Early – Launch July 2029			Primary – Launch May 2031			Secondary – Launch May 2033		
	$P_{L,1AU}$ $[kW]$	$N_{s/c}$ $[-]$	δb $[\%\ C]$	$P_{L,1AU}$ $[kW]$	$N_{s/c}$ $[-]$	δb $[\%\ C]$	$P_{L,1AU}$ $[kW]$	$N_{s/c}$ $[-]$	δb $[\%\ C]$
Lowest Mass	86.78	**1**	**154.71**	89.26	**1**	**126.43**	88.74	**2**	**133.90**
50th percentile	86.92	**1**	**78.83**	89.56	**2**	**118.21**	89.86	**3**	**99.28**
Highest Mass	87.10	**2**	**89.57**	88.78	**3**	**104.54**	88.50	**4**	**76.16**

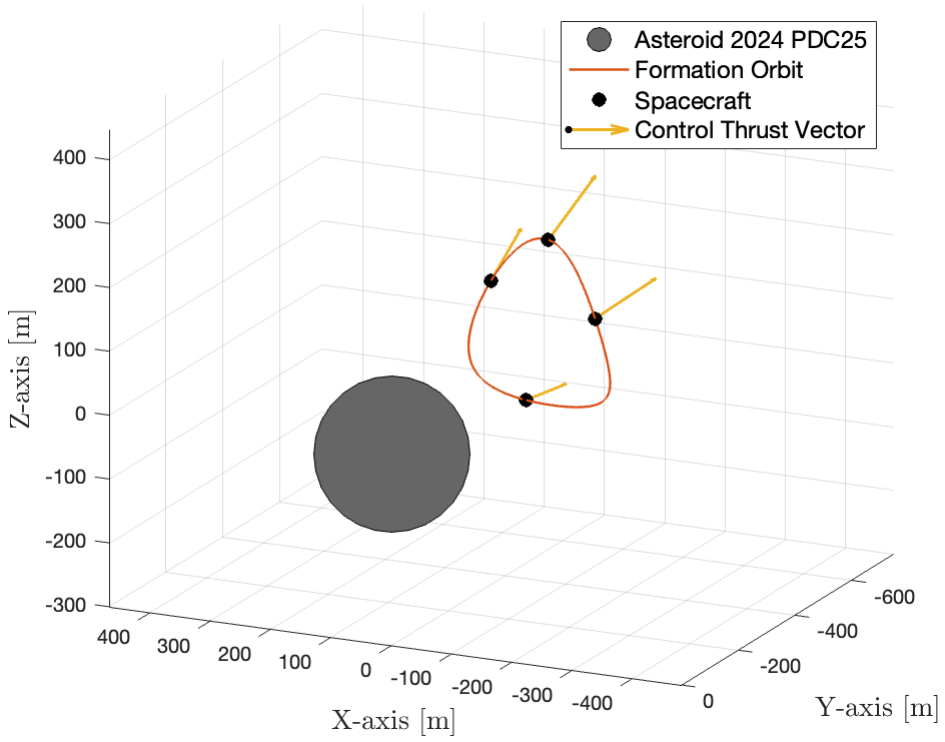

Highest Mass case
Secondary mission

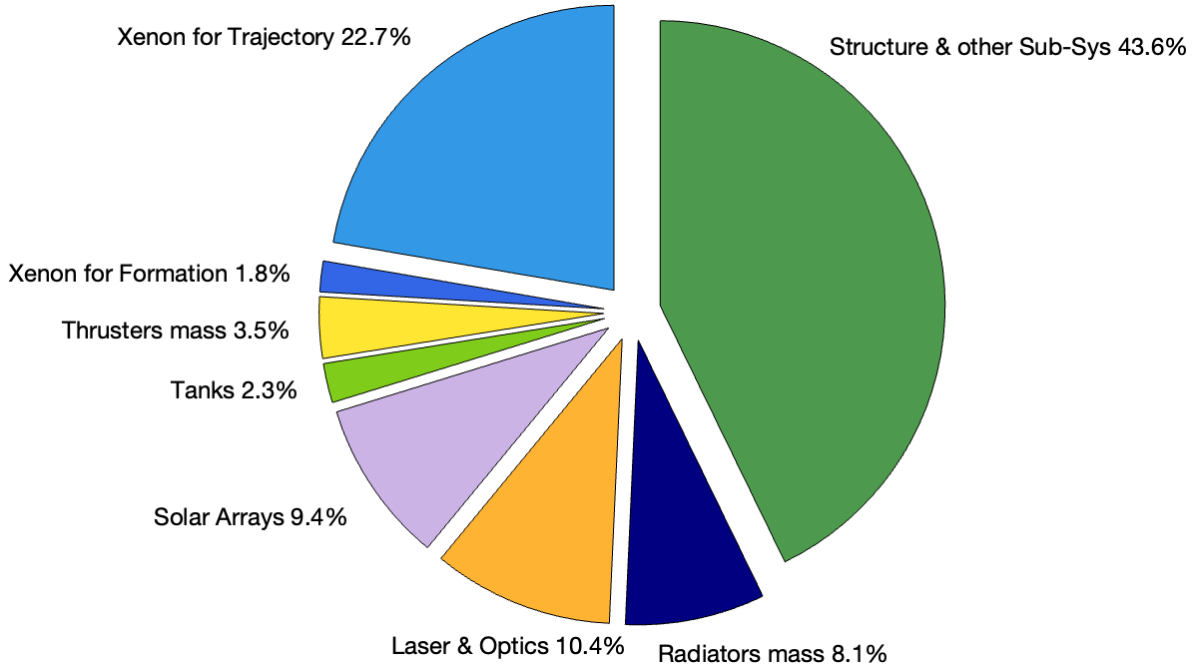

Multiple LA – Early, Primary & Secondary missions

	Launch	Arrival	ToF $[days]$	C_3 $[km^2/s^2]$	m_{s/c_0} $[kg]$	$m_{f_{LT}}$ $[kg]$	$P_{L,1AU}$ $[kW]$	$N_{s/c}$ $[-]$	δb $[\%\ C]$
Lowest Mass	2029-07-26	2031-05-22	664.84	24.22	8890.63	1970.47	86.78	**1**	**154.71**
	2031-05-08	2032-10-19	530.70	19.22	8844.72	1572.89	89.26	**1**	**126.43**
	2033-05-03	2034-12-17	592.31	19.13	9760.07	1755.49	88.74	**2**	**133.90**
50th percentile	2029-07-26	2031-05-14	657.23	22.22	8590.63	1947.91	86.78	**1**	**78.83**
	2031-05-08	2032-11-29	571.21	21.10	9402.47	1692.96	89.56	**2**	**118.21**
	2033-05-03	2035-01-02	608.75	24.84	8931.31	1804.23	89.86	**3**	**99.28**
Highest Mass	2029-07-26	2031-05-17	660.22	23.98	8664.85	1956.76	87.10	**2**	**89.57**
	2031-05-08	2032-11-05	547.00	24.70	8364.90	1621.19	88.78	**3**	**104.54**
	2033-05-03	2034-12-23	598.66	24.60	8478.73	1774.30	88.50	**4**	**76.16**

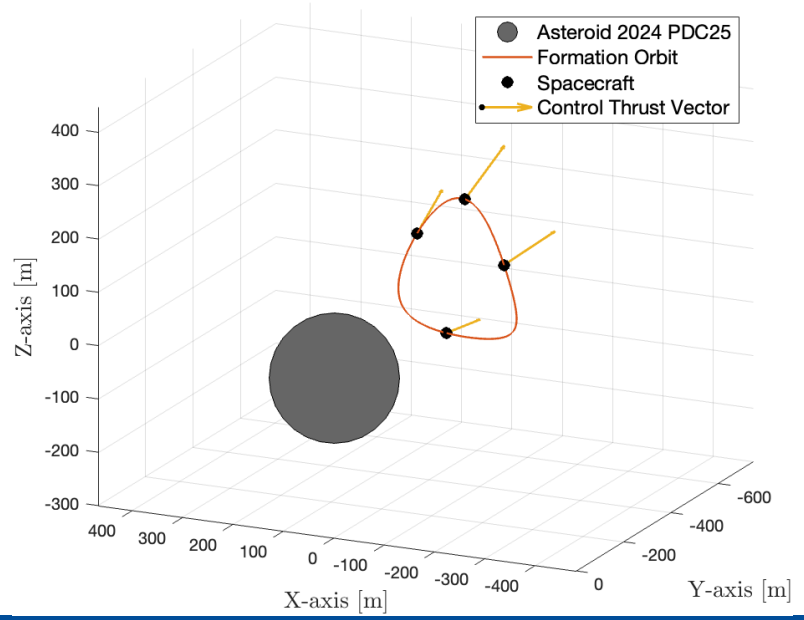

Highest Mass case
Secondary mission

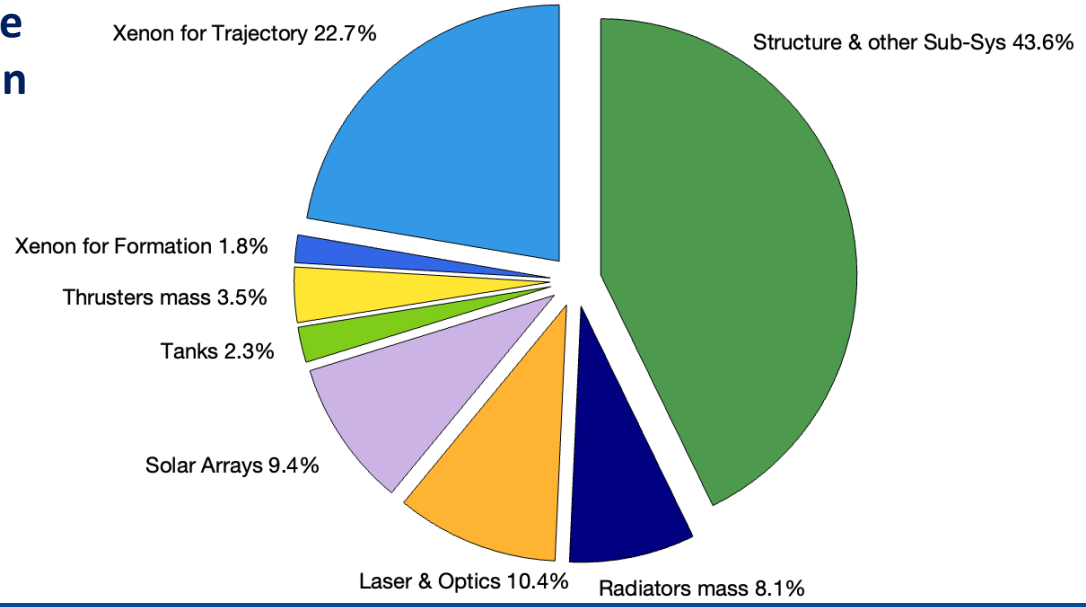

Standard and Enhanced Gravity Tractor

- Spacecraft hovers near the asteroid with thrusters angled outward [12].
- **Mutual gravitational attraction** → Small but continous acceleration.

$$a_{GT}(t) = \frac{G\, m_{s/c}(t)}{d_{hover}^2}$$

$$a_{EGT}(t) = \frac{G\, [m_{s/c}(t) + M_{gain}]}{d_{hov,EGT}^2}$$

- **The Enhanced Gravity Tractor (EGT)** collects material from the asteroid surface to increase the spacecraft mass [13].

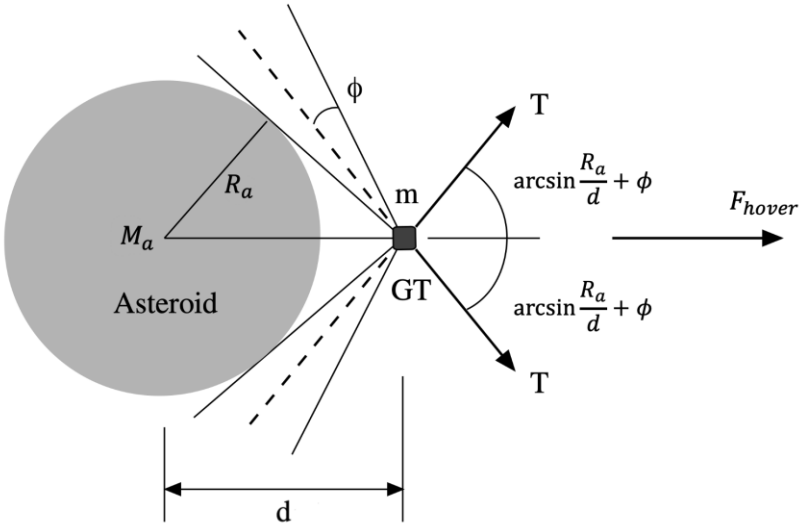

Geometry of gravity tractor hovering [12].

Close-proximity operations

Collected mass
$M_{gain} = 50 \times 10^3\ kg$

Fuel allowance
5% of m_{s/c_0}

One-month
period after arrival

Perturbing acceleration in TNH frame:

- $\boldsymbol{a}(t) = [\pm a_{GT}(t)\ \ 0\ \ 0]^T$
- $\boldsymbol{a}(t) = [\pm a_{EGT}(t)\ \ 0\ \ 0]^T$

No additional optimisation variables

[12] B. Wie, Journal of guidance, control, and dynamics, vol. 31, no. 5, pp. 1413–1423, 2008. DOI: https://doi.org/10.2514/1.32735.
[13] D.D. Mazanek et al., IAA Planetary Defense Conference, Frascati, Italy, 2015. IAA-PDC-15-04-11. URL: https://ntrs.nasa.gov/citations/20150010968.

Standard GT – Early & Primary campaigns

	Launch	Arrival	ToF $[days]$	C_3 $[km^2/s^2]$	m_{s/c_0} $[kg]$	$m_{f_{LT}}$ $[kg]$	$m_{f_{hover}}$ $[kg]$	d_{hover} $[m]$	δb [% C]
Lowest Mass	2029-06-16	2031-06-30	743.12	10.77	11479.84	2202.47	2945.20	85.74	**51.49**
	2031-06-06	2033-07-19	774.27	10.58	11261.59	2294.79	2406.47	85.29	**31.75**
50th percentile	2029-06-16	2031-08-01	775.65	11.21	11527.79	2298.86	2920.50	99.69	**37.40**
	2031-06-06	2033-11-15	892.83	10.99	11624.61	2646.19	2320.64	98.99	**22.26**
Highest Mass	2029-06-06	2031-11-12	889.37	12.07	11853.85	2635.93	2850.10	119.95	**24.87**
	2031-06-06	2033-06-15	739.95	10.44	11937.57	2193.08	2460.63	122.20	**17.28**

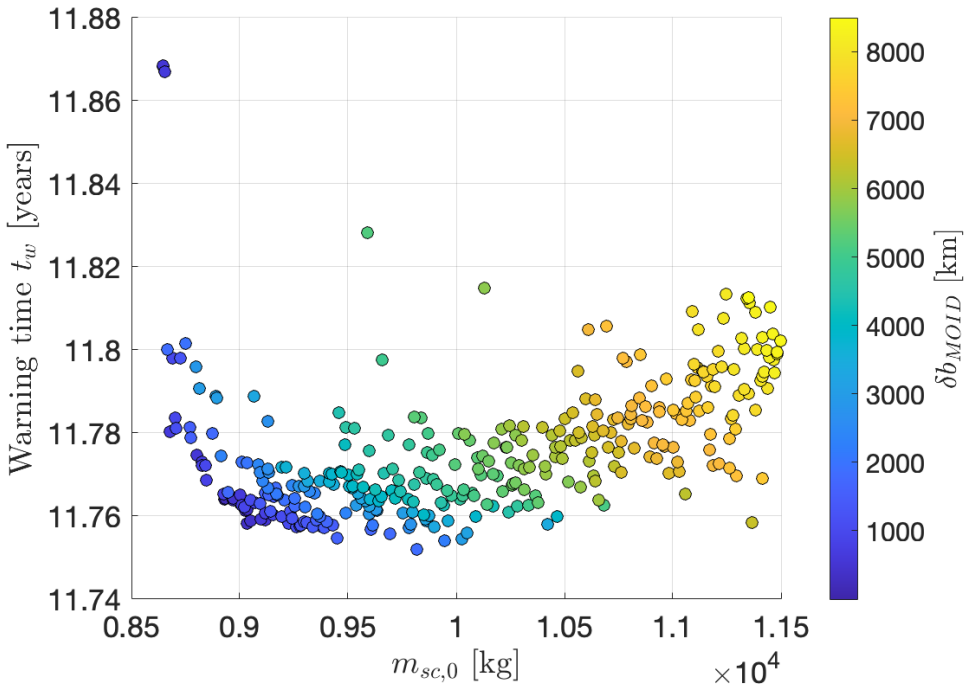

50th percentile
Early mission

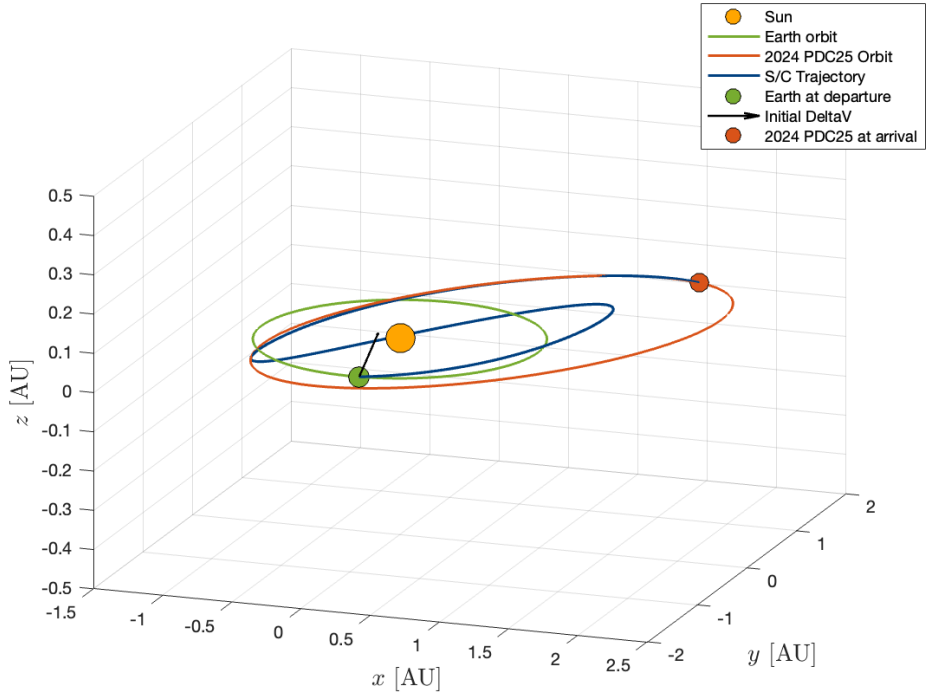

Enhanced GT – Early & Primary campaigns

	Launch	Arrival	ToF $[days]$	C_3 $[km^2/s^2]$	m_{s/c_0} $[kg]$	$m_{f_{LT}}$ $[kg]$	$m_{f_{hover}}$ $[kg]$	$d_{hover,EGT}$ $[m]$	δb [% C]
Lowest Mass	2029-06-16	2031-04-20	672.99	14.34	11018.16	1994.63	3475.42	147.17	**124.32**
	2031-06-06	2033-03-20	653.42	11.63	10500.33	1936.62	2820.91	146.74	**80.52**
50th percentile	2029-06-16	2031-06-10	723.21	11.01	11401.28	2143.46	3429.11	196.92	**68.05**
	2031-06-06	2033-03-09	642.06	10.71	10047.23	1902.95	2831.10	195.36	**45.51**
Highest Mass	2029-06-16	2031-04-29	681.99	12.98	11102.06	2021.29	3467.15	256.70	**40.70**
	2031-06-06	2033-03-07	640.25	10.60	10129.78	1897.56	2832.91	255.07	**26.78**

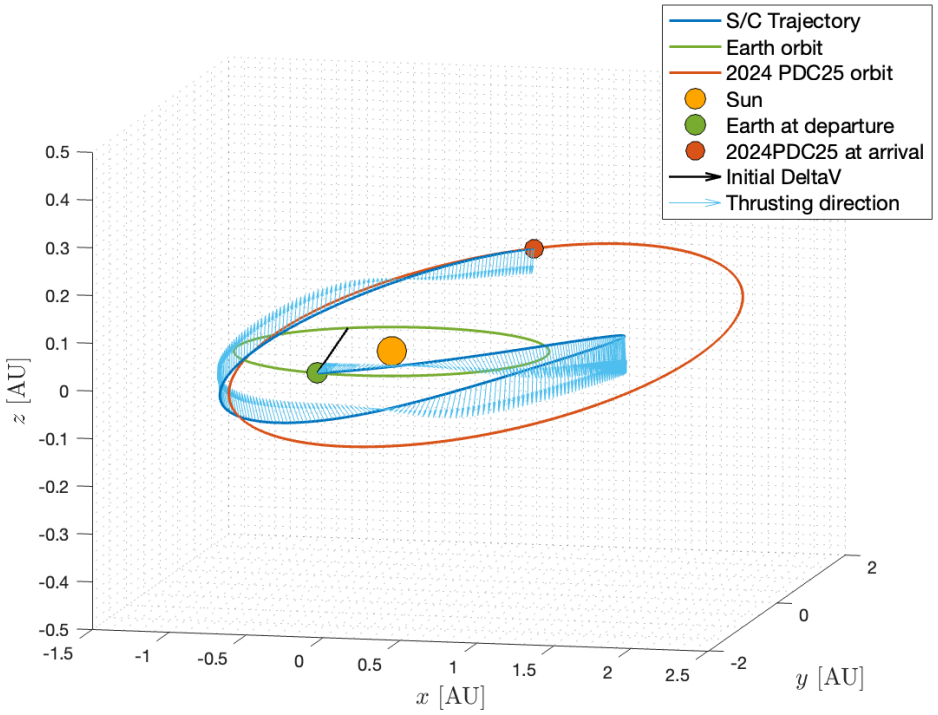

Highest Mass case
Primary mission

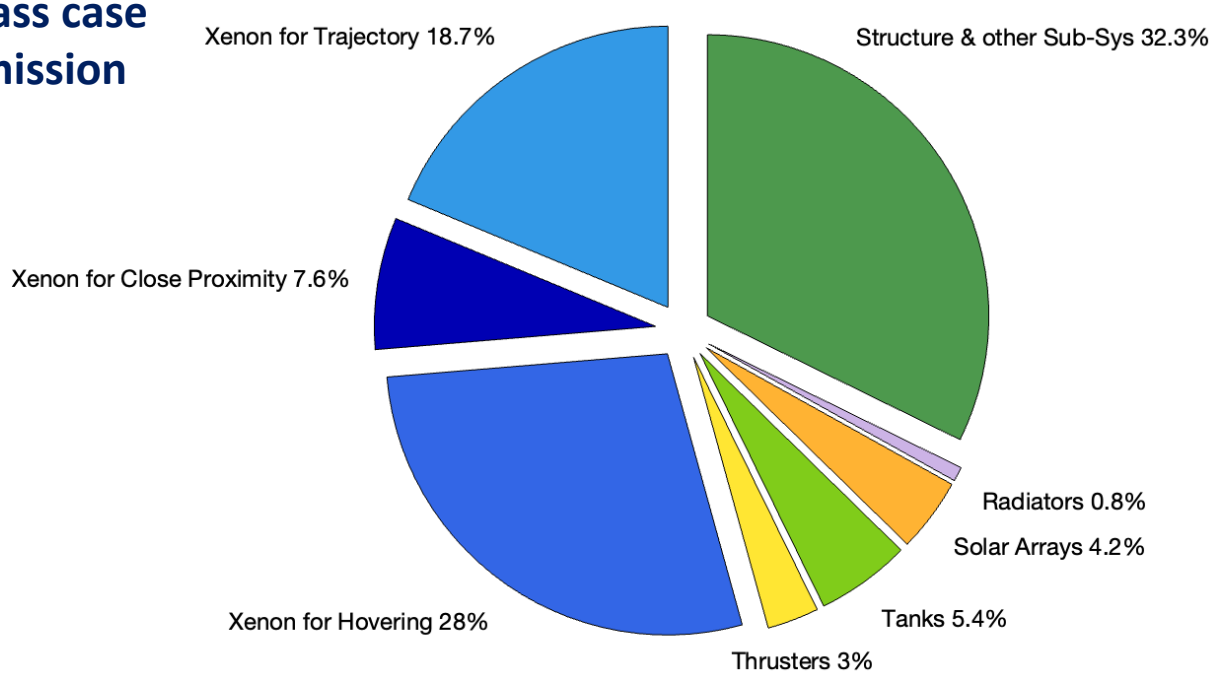

Key results and TRL considerations

Standard GT	Enhanced GT
• High TRL	• High performance
• Low performance	• Low TRL

SLA hovering	MLA in Formation Flight
• Low TRL	• High performance
• Low performance	• Low TRL

Stand-off NEDs in "Carrier" configuration

- High TRL
- Up to 13 impulses
- Political and legal limitations

Mission	Perihelion	N_{NEDs} [−]
Early	1st November 2032	5
Primary	15th December 2034	5-7
Secondary	27th January 2037	7-9
Late	12th March 2039	13

Single and Multiple IBD

- High Performance
- Increasing TRL

Mission	Launch	$N_{s/c}$ [−]	Development time
Early	June 2029	1	Stringent
Primary	May 2031	2-3	Sufficient
Secondary	June 2033	3-6	Extensive

This project has received funding from the European Research Council (ERC) under the European Union's Horizon Europe research and innovation programme (grant agreement No 101089265 – GREEN SPECIES)

ANALYSIS OF ASTEROID DEFLECTION MISSION OPTIONS FOR THE 2025 PLANETARY DEFENSE CONFERENCE HYPOTHETICAL ASTEROID IMPACT THREAT SCENARIO BY THE ITALIAN SPACE AGENCY DELEGATION AT SMPAG

S. Franzese, E. Basile, E. M. Polli, C. Colombo, P. Vasiliki, M. Castronuovo, J. L. Cano

POLITECNICO MILANO 1863

Planetary Defence Conference 2025 - 6th May 2025